Interlayer Exchange Coupling in Asymmetric Co-Fe/Ru/Co-Fe Trilayers Investigated with Broadband Temperature-Dependent Ferromagnetic Resonance

Behrouz Khodadadi, Jamileh Beik Mohammadi, Joshua Michael Jones, Abhishek Srivastava, Claudia Mewes, Tim Mewes, and Christian Kaiser

Phys. Rev. Applied **8**, 014024 — Published 24 July 2017

DOI: 10.1103/PhysRevApplied.8.014024

Broadband and temperature dependent ferromagnetic resonance investigation of interlayer exchange coupling in asymmetric $CoFe/Ru(x)/CoFe$ trilayers

Behrouz Khodadadi,[1,2] Jamileh Beik Mohammadi[1,2], Joshua Michael Jones[1,2] , Abhishek Srivastava, [1,2] Claudia Mewes,[1,2] Tim Mewes,[1,2] Christian Kaiser [3]

[1]*Department of Physics and Astronomy, The University of Alabama, Tuscaloosa, Alabama 35487, USA*

[2] *Center for Materials for Information Technology (MINT), The University of Alabama, Tuscaloosa, Alabama 35487, USA*

[3] *Western Digital, 44100 Osgood Road, Fremont, California 94539, USA*

Keywords: Interlayer exchange-coupled trilayer, frequency dependence of coupling field, temperature dependence of coupling field

Abstract:

We report on a comprehensive study of the interlayer exchange coupling in CoFe(5nm)/Ru(x)/CoFe(8nm) trilayers (x=0.8…2.8 nm), using broadband ferromagnetic resonance. A systematic frequency dependence of the field separation between the acoustic and optic modes is found, which is caused by different effective magnetizations of the two ferromagnetic layers. Hence, it is shown that the broadband measurements are vital for reducing the systematic error margins in the determination of interlayer exchange coupling using ferromagnetic resonance. We have also investigated the temperature dependence of the interlayer exchange coupling and compare our results with existing theories. It is shown that models which take into account the temperature dependence due to thermal excitations of spin waves within the ferromagnetic layers, have a considerably better agreement with the experiment than models solely based on spacer and interface contributions to the temperature dependence.

I. Introduction

There have been extensive experimental and theoretical studies through the last decades on interlayer exchange-coupled (IEC) systems consisting of two ferromagnetic layers coupled through a nonmagnetic spacer layer[1-4]. Different theoretical models have been developed to explain the oscillatory behavior based on the characteristics of the Fermi surface of the spacer layer[5, 6] or using the spin dependent scattering of the Bloch waves at the ferromagnetic-spacer layer interface.[7] The interlayer exchange coupling was first discovered in 1986 for Fe/Cr/Fe, Gd/Y/Gd and Dy/Y/Dy structures.[8-10] This was followed by the discovery of Giant Magneto-Resistance (GMR) effect in the interlayer exchanged-coupled Fe/Cr/Fe systems that gave birth to spin dependent transport phenomena. Furthermore, interlayer exchange-coupled layers with a strong antiferromagnetic coupling in combination with an exchange-biased layer have also been extensively used as synthetic antiferromagnets in read head sensors in the magnetic recording industry. For the development of new magnetic recording technologies such as Heat Assisted Magnetic Recording (HAMR) but also for the emerging spin transfer torque based memories[11], obtaining a better understanding of the physical mechanisms that determine the temperature dependence of the interlayer exchange coupling remains an important goal.

Ferromagnetic resonance (FMR) is an excellent tool for quantitative determination of the interlayer exchange coupling for both ferromagnetically and antiferromagnetically coupled systems. Two different resonances are observed in the FMR spectra of the IEC structures[12,13]. For the acoustic mode, both layers precess in-phase whereas for the optic mode they precess out-of-phase[11, 12]. However, for two identical interlayer exchange coupled ferromagnetic layers, the intensity of the optical mode is zero and therefore cannot be detected using FMR[14-16]. A common approach to circumvent this difficulty is therefore to use an asymmetric trilayer system, for

example by using ferromagnets with different film thicknesses. In this paper, we utilize broadband FMR to show that the mode separation, used for experimental determination of the interlayer exchange coupling, has a noticeable frequency dependence in asymmetric IEC systems where the two ferromagnetic layers are of different thicknesses. This frequency dependence arises from the difference in the effective magnetizations of the ferromagnetic layers[17]. Hence for the experimental determination of the coupling strength, it is very important to have broadband ferromagnetic resonance data to avoid uncertainties for the interlayer exchange coupling strength, caused by the frequency dependence of the mode separation.

We have performed a comprehensive experimental temperature dependent investigation of the interlayer exchange coupling strengths which enable us to compare them with the predictions of different theoretical models, and thereby provides new information about the physical origin of the temperature dependence.

II. Experimental Procedures

The samples were fabricated using magnetron sputter deposition on SiO_2 substrates having the following layer sequence $SiO_2/Ta(3nm)/Ru(2nm)/Co_{90}Fe_{10}(5nm)/Ru(t)/Co_{90}Fe_{10}(8nm)/Ru(3nm)/Ta(3nm)/Ru(3nm)$. The thickness t of the Ru layer varied from 0.8nm to 2.8 nm. The ferromagnetic resonance properties of the samples were measured using a custom designed broadband ferromagnetic resonance setup which uses a coplanar waveguide for microwave excitation and operates in the $1-65\ GHz$ frequency range[18-22] .At a fixed microwave frequency, the external magnetic field is swept through the resonance field of the sample. The microwave loss at the resonance condition can be detected by measuring the transmitted microwave power through the sample. The setup was also used with a closed cycle cryostat for temperature dependent measurements[23].

III. Model

a) Determination of interlayer exchange coupling field by ferromagnetic resonance

For a trilayer system of two ferromagnetic layers separated by a non-magnetic spacer the interlayer exchange coupling, also known as RKKY coupling, results in two resonance modes of the system referred to as the acoustic and optic modes[1, 4]. The acoustic mode corresponds to the in-phase and the optic mode to the out-of-phase precession of the ferromagnetic layers, see figure 1. For a symmetric trilayer, equation (1) describes the resonance frequencies for the acoustic and optic mode

$$f = \gamma' \sqrt{\left(H_{res,ac}\right)\left(H_{res,ac} + 4\pi M_{eff}\right)} \quad (1)$$

$$f = \gamma' \sqrt{\left(H_{res,op} + 2H_{ex}\right)\left(H_{res,op} + 2H_{ex} + 4\pi M_{eff}\right)}$$

Here the external magnetic field is applied in the film plane, H_{ex} is the interlayer exchange coupling field and M_{eff} is the effective magnetization, which for a symmetric trilayer is identical for both layers. Due to the oscillating nature of the RKKY interaction the coupling between the two ferromagnetic layers changes sign with changing interlayer thickness between ferromagnetic $H_{ex} > 0$ and antiferromagnetic $H_{ex} < 0$. As seen in equation (1) the optic mode is shifted along the field axis by twice the exchange field as compared to the acoustic mode. Moreover, the resonance condition for the acoustic mode is identical to the resonance condition for a single layer thin film. Therefore, in a symmetric trilayer structure, the exchange field is equal to half of the field separation between the two modes. However, in a typical ferromagnetic resonance measurement, the microwave magnetic field profile is homogeneous over the thin film structure, hence it is difficult to excite the optic mode in a symmetric trilayer[24]. One approach to overcome this difficulty is to use asymmetric trilayers, i.e. two ferromagnetic layers of different thicknesses,

or different saturation magnetizations. In this case, solving the LLG equation leads to a more complicated dispersion relation as compared to the symmetric case.

Following the work of Zhang et al.[13], we use the following expression for the free energy density of an asymmetric exchange-coupled trilayer

$$E = \sum_{i=1}^{2} t_i \left[-M_s H_0 (\cos\theta_H \cos\theta_i + \sin\theta_H \sin\theta_i \cos\varphi_i) - \frac{1}{2} 4\pi M_{eff,i} M_s \sin^2\theta_i \right] \quad (2)$$
$$+ J_{inter} [\cos\theta_1 \cos\theta_2 + \sin\theta_1 \sin\theta_2 \cos(\varphi_1 - \varphi_2)]$$

Here θ_i and φ_i are the polar and azimuthal angles of the magnetization vectors of the ferromagnetic layers at equilibrium, see figure 2. Also θ_H is the polar angle of the external magnetic field which $\theta_H = \frac{\pi}{2}$ in our configuration, see figure 2. Furthermore, J_{inter} is the effective coupling constant with units of energy/area and $4\pi M_{eff,i}$ includes both demagnetization and perpendicular anisotropy fields and is defined as[19, 23, 25]

$$4\pi M_{eff,i} = 4\pi M_s - 2\frac{K_{u,i}}{M_s} \quad (3)$$

where $K_{u,i}$ is the out-of-plane anisotropy constant. Here, $K_{u,i} > 0$ indicates that the easy axis of the perpendicular magnetic anisotropy energy is along the film normal, whereas $K_{u,i} < 0$ corresponds to an easy plane in the film plane. In the case of thin films with no bulk contribution to the out-of-plane anisotropy, one has $K_{u,i} = \frac{2k_i}{t_i}$, where k_i is the average interfacial perpendicular anisotropy of layer i and t_i is its thickness. Therefore, the value of $K_{u,i}$ will generally be different for two FM layers of different thickness. Note that no higher order out-of-plane anisotropy or in-plane magnetic anisotropy fields are included in equation (2). Using the above energy density the resonance frequencies of the acoustic and optic modes are found by the

following equation

$$\left(\frac{f}{\gamma'}\right)^4 - b\left(\frac{f}{\gamma'}\right)^2 + c = 0 \quad (4)$$

Where b and c are defined as follows[13]

$$b = \frac{E_{\theta_1\theta_1}E_{\varphi_1\varphi_1} - {E_{\theta_1\varphi_1}}^2}{t_1^2 M_s^2 \sin^2\theta_1} + \frac{E_{\theta_2\theta_2}E_{\varphi_2\varphi_2} - {E_{\theta_2\varphi_2}}^2}{t_2^2 M_s^2 \sin^2\theta_2} + 2\frac{E_{\theta_1\theta_2}E_{\varphi_1\varphi_2} - E_{\theta_1\varphi_2}E_{\theta_2\varphi_1}}{t_1 t_2 M_s^2 \sin\theta_1 \sin\theta_2} \quad (5)$$

$$\begin{aligned} c = \frac{1}{t_1^2 t_2^2 M_s^4 \sin^2\theta_1 \sin^2\theta_2} [& {E_{\theta_1\theta_2}}^2 {E_{\varphi_1\varphi_2}}^2 + {E_{\theta_1\varphi_1}}^2 {E_{\theta_2\varphi_2}}^2 + {E_{\theta_1\varphi_2}}^2 {E_{\theta_2\varphi_1}}^2 - {E_{\theta_1\theta_2}}^2 E_{\varphi_1\varphi_1}E_{\varphi_2\varphi_2} \\ & - {E_{\varphi_1\varphi_2}}^2 E_{\theta_1\theta_1}E_{\theta_2\theta_2} - {E_{\theta_1\varphi_1}}^2 E_{\theta_2\theta_2}E_{\varphi_2\varphi_2} - {E_{\theta_1\varphi_2}}^2 E_{\theta_2\theta_2}E_{\varphi_2\varphi_2} - {E_{\theta_2\varphi_1}}^2 E_{\theta_1\theta_1}E_{\varphi_1\varphi_1} \\ & + E_{\theta_1\theta_1}E_{\varphi_1\varphi_1}E_{\theta_2\theta_2}E_{\varphi_2\varphi_2} + 2E_{\theta_1\theta_1}E_{\varphi_1\varphi_2}E_{\theta_2\varphi_2}E_{\theta_2\varphi_2} + 2E_{\theta_1\varphi_1}E_{\theta_1\varphi_2}E_{\varphi_1\varphi_2}E_{\theta_2\theta_2} \\ & + 2E_{\theta_1\theta_2}E_{\theta_1\varphi_2}E_{\varphi_1\varphi_2}E_{\theta_2\varphi_2} \\ & + 2E_{\theta_1\theta_2}E_{\theta_1\varphi_1}E_{\theta_2\varphi_1}E_{\varphi_2\varphi_2} - 2E_{\theta_1\varphi_1}E_{\theta_2\varphi_2}\left(E_{\theta_1\theta_2}E_{\varphi_1\varphi_2} + E_{\theta_1\varphi_2}E_{\theta_2\varphi_1}\right) \\ & - 2E_{\theta_1\theta_2}E_{\varphi_1\varphi_2}E_{\theta_1\varphi_2}E_{\theta_2\varphi_1}] \end{aligned}$$

Where $E_{\theta\phi}$ are the partial derivatives of the free energy density E with respect to the magnetization angles at equilibrium, and M_s is the saturation magnetization which for simplicity is assumed to be the same for the two layers.

b) Temperature dependence of coupling field

While the origin of the interlayer exchange coupling has been studied in detail and is considered to be well understood[4, 7, 8] , the origin of its temperature dependence remains an open question[26-29]. Here we briefly summarize the theoretical mechanisms that have been proposed in the literature to explain the reduction of the interlayer exchange coupling at finite temperature. A detailed discussion can be found in the work by Schwieger and Nolting[26, 27]

i. Spacer contribution and interface contributions

As first proposed by Bruno[5, 7, 30] and Edwards[31] the broadening of the Fermi edge in the **spacer layer** will lead to a temperature dependence of the interlayer exchange coupling.

Furthermore, the phase and magnitude of the complex reflection coefficients at the **interface** between ferromagnet and the spacer layer may also be temperature dependent.

The temperature dependence of the interlayer exchange coupling resulting from the spacer and interface contribution can be written as[27]

$$\tilde{J}_{inter} = \sum_{\alpha} \tilde{J}^{\alpha}_{inter}(t, T = 0)\, f^{\alpha}(d, T) \tag{6}$$

Where α counts the number of stationary Fermi surface vectors relevant for the interlayer exchange coupling[30, 32] and d is the spacer layer thickness. Note that similar to the notation in reference[27], $\tilde{J}_{inter}$ in equation (6) has units of energy. The temperature dependent functions are

$$f^{\alpha} = \frac{c_{\alpha} T}{\sinh(c_{\alpha} T)} \tag{7}$$

Where

$$c_{\alpha} = \frac{2\pi k_B}{\hbar v_f^{\alpha}} d + 2\pi k_B D_{\phi}^{\alpha} \tag{8}$$

Here the first and second terms on the RHS of equation (8) represent the spacer and interface contributions respectively, also v_f^{α} is the Fermi velocity and $D_{\phi}^{\alpha} = \frac{d\phi^{\alpha}}{d\varepsilon}_{\varepsilon=\varepsilon_f}$, where ϕ^{α} is the phase of reflection coefficient : $\Delta r^{\alpha} = |r^{\alpha}| e^{i\phi\alpha}$. For interlayer exchange coupling determined by a single Fermi surface vector, one has

$$\frac{\tilde{J}_{inter}(T)}{\tilde{J}_{inter}(0)} = \frac{cT}{\sinh(cT)} \tag{9}$$

ii. Spin wave excitations

Another mechanism that can contribute to the temperature dependence of the interlayer exchange interaction are spin wave excitations in the magnetic layers[17, 26, 27, 33]

$$\frac{\tilde{J}_{inter}(T)}{\tilde{J}_{inter}(0)} = 1 - \frac{1}{8\pi J S^2 \tilde{J}_{inter}(0)} (k_B T)^2 \sum(T) \qquad (10)$$

$$\sum(T) = \sum_{n=1}^{\infty} \frac{1}{n^2} e^{-\beta g \mu_B B n} \left(1 - e^{-\frac{1}{S}\tilde{J}_{inter}(0)\beta n}\right), where \quad \beta = \frac{S}{k_B T}$$

Where S is the spin quantum number and B is the magnetic induction. Note that J , which appears in the denominator of the first part of equation (10), denotes the intra-layer exchange coupling constant[27]. According to equation (10), the interlayer exchange coupling is expected to decrease with temperature faster than $1 - xT$ but slower than $1 - xT^2$, see reference[27].

As pointed out by Schwieger and Nolting[27] over the experimentally accessible temperature range, all three mechanisms can be approximated as

$$f(T) = \frac{\tilde{J}_{inter}(T)}{\tilde{J}_{inter}(0)} \approx 1 - xT^y \,, 1 < y < 2 \qquad (11)$$

Where the exponent y is expected to be in the range from 1 to 2 and is often assumed to be 1.5[18-21]. The fact that all three contributions can be approximated by this power law, explains the difficulty to distinguish them solely based on the temperature dependence of the interlayer exchange coupling. However, the dependence of $f(T)$ on the spacer thickness can provide valuable insights. For the spacer contribution, one expects a linear increase of the parameter c in equation (8) with the spacer thickness d. The interface contribution on the other hand, is independent of the spacer thickness, see equation (8). The contribution due to the spin wave

excitations shows a weak implicit dependence that oscillates with the spacer thickness[26, 27], this model predicts a more pronounced temperature dependence for small coupling fields.

IV. Numerical results

Equation (4) was solved numerically in the 0-20 kOe interval to determine the resonance frequencies of both acoustic and optic modes at each magnetic field point for an asymmetric IEC trilayer. The gyromagnetic ratio γ' was 3.03 GHz/kOe for both layers, and the effective magnetization M_{eff} was set to 1300 emu/cm^3 and 1400 emu/cm^3 for the 5nm and 8nm CoFe layers, respectively. These parameters were selected in the light of experimental values of gyromagnetic ratio and effective magnetization for a CoFe(13nm) single layer, which are equal to 3.03 GHz/kOe and 1420 emu/cm^3 respectively, see section V. The simulated frequency versus resonance field plots are shown in figure 3 for coupling field values of -400 Oe (a), -100 Oe (b), 0 Oe (c), 100 Oe (d) and 400 Oe (e), where the negative sign refers to antiferromagnetic coupling. Note that, for simplicity the saturation magnetization of both layers was assumed to be the same value, but a small interfacial perpendicular magnetic anisotropy was assumed, which leads to the different effective magnetization values for the 5 nm (1300 emu/cm^3) and 8 nm CoFe (1400 emu/cm^3). We point out that for asymmetric trilayers, we define the interlayer exchange coupling field as[13]

$$H_{ex} = \frac{1}{2}\frac{(t_1 + t_2)J_{inter}}{M_s t_1 t_2} \quad (12)$$

i.e. the effective interlayer exchange field is equal to the arithmetic mean of the exchange field values for each FM layer, $H_{ex,i} = \frac{J_{12}}{M_s t_i}$. Figure 4(a) shows the frequency dependence of the field separation between the acoustic and optic modes that is found from the numerical frequency versus resonance field plots shown in figure 3. As can be expected, the difference of the effective

magnetizations of the two layers leads to a frequency dependence of the mode separation. As shown in figure 4(b) this frequency dependence of the mode separation vanishes for two FM layers with equal effective magnetization. Therefore, broadband ferromagnetic resonance measurements are required to reliably extract the interlayer exchange coupling of trilayers for which the assumption of equal effective magnetizations cannot be supported using independent measurements. As will be shown below fitting of broadband FMR data enables the precise determination of the interlayer exchange coupling and the effective magnetizations of the trilayers.

V. Experimental results

a) Frequency dependence of the mode separation

Figure 5 shows the experimental raw FMR signals at 20 GHz for the CoFe(5 nm)/Ru(0.8 nm)/CoFe (8 nm) (figure 5(a)) and CoFe(5 nm)/Ru(2 nm)/CoFe(8 nm) (figure 5(c)) samples with anti-ferromagnetic interlayer exchange coupling and CoFe(5 nm)/Ru(1.4 nm)/CoFe (8 nm) (figure 5(b)) and CoFe(5 nm)/Ru(2.6nm)/CoFe(8 nm) (figure 5(d)) samples, which show ferromagnetic interlayer exchange coupling.

Figures 6 shows the broadband experimental Kittel plots for the same samples as in figure 5, which enables us to determine the $H_{res,ac} - H_{res,op}$ between the acoustic and optic modes. As shown in figure 7 the experimental field separation data show the same trend as a function of frequency as the numerical simulations discussed in the previous section. In order to accurately, determine the coupling field, the experimental H_{res} versus frequency data for both modes were fitted with the full numerical model using equation (2) as shown in figures 6(a)-(d) and 7 for exemplary AF and FM coupled samples. This approach minimizes systematic errors caused by the frequency dependence of the mode separation and is used to determine the

experimental value of the interlayer exchange coupling field H_{ex} for all samples. To illustrate this consider the $CoFe(5\text{ nm})/Ru(2\ nm)/CoFe(8\text{ nm})$ sample, here the fit using the full model results in an interlayer exchange coupling field of $H_{ex} = -250 \pm 3\ Oe$. If one instead uses half the field separation of the two resonances at 50GHz, as implied by equation (1), one would obtain a value for the interlayer exchange coupling field of $H_{ex} = -367\ Oe$. This value differs by almost 47% from the value determined using the full model. Because this approach takes into account data collected over a wide frequency range the error margins are very small, see figure 7. Determining meaningful error margins for the interlayer exchange field determined from the field separation at a single frequency would also be challenging. When fitting broadband data using the full model on the other hand one can determine the statistical error margins by calculating the approximation of the Hessian matrix and its inverse at the convergence point[34].

To conclude, we have shown that in asymmetric trilayers the interlayer exchange coupling is not solely responsible for the field separation between the optic and acoustic modes, as differences between the effective magnetizations of the ferromagnetic layers will also influence the mode separation. Broadband measurements enabled us to identify and distinguish between these two contributions.

b) Temperature dependence of the coupling field

In addition to the room temperature experiments, a comprehensive set of broadband ferromagnetic resonance measurements were performed at lower temperatures down to 10 K.

Figure 8 shows exemplary experimental broadband temperature dependent data for the samples with Ru thicknesses of 0.8 nm and 1.2 nm. The data were fitted using the full numerical model to determine the interlayer exchange coupling field at each temperature. Figure 9 shows the

experimentally determined interlayer exchange coupling field as a function of Ru thickness at different temperatures. The strongest antiferromagnetic coupling is observed for the sample with the smallest Ru thickness of $0.8\ nm$ and the first transition from antiferromagnetic coupling to ferromagnetic coupling happens between 1 nm and 1.2 nm and the second transition from AF to FM coupling takes place between 2 nm and 2.4 nm. The strongest ferromagnetic coupling is observed at a thickness of 1.2 nm with the second antiferromagnetic and ferromagnetic peaks occurring at 1.8 nm and 2 nm respectively, and the coupling cross over from ferromagnetic to antiferromagnetic happening between 1.4 nm and 1.8 nm. In accordance with all three theoretical models, the oscillation amplitude (coupling field) increases noticeably with decreasing temperature while the oscillation period remains unchanged[13, 30]. The period of oscillation is approximately 1.1 nm which is consistent with the reported value for Co/Ru superlattice structures[35].

In order to compare our experimental results with the theoretical predictions for the temperature dependence discussed in section III(b), we determine the interlayer exchange coupling constant J_{inter} using equation (12). Here we use $M_s = 1600\ \mathrm{emu/cm^3}$ for all temperatures, as the changes in M_s are expected to be small in accessible temperature range. Note that the Curie temperature of CoFe alloys are very high, close to 1000 °C[36, 37].

Figure 10 shows the temperature dependence of the coupling constant for the samples with Ru thicknesses of 0.8 nm and 1.2 nm and the fits to the experimental data using equations (9) and (11). Note that the uncertainties of the coupling constant J_{inter} values were calculated using equation (12) and the standard deviations of the numerically fitted values of H_{ex}, while considering 5% error margin in the values of saturation magnetization and thicknesses of the

CoFe layers. As shown in figure 10 both equations (9) and (11) result in a reasonable agreement with the experimental data and a similar fit quality.

As discussed in section III despite the difficulties in distinguishing between the existing theoretical models caused by their similar temperature dependence, one can obtain further insights by investigating the influence of the spacer layer thickness, magnitude and sign of the interlayer exchange coupling on the temperature dependence of the model parameters. When comparing the spacer and interface models as described by equation (9) and the more generally applicable approximation given by equation (11) one notes that, the fit parameter x is highly correlated to fit parameter c [27], which itself is supposed to scale linearly with the spacer layer thickness based on the spacer model, see equation (8). As shown in figure 11 no such dependency is seen for the fit parameters c or x. On the other hand, the oscillatory behavior of both fit parameters; which is more pronounced in the case of the c parameter; follows the oscillatory behavior of the exchange field as a function of the spacer layer thickness which is consistent with the prediction of the spin wave excitation model.

In summary, a frequency dependence was found in the FMR mode separation of asymmetric interlayer exchange coupled CoFe/Ru(x)/CoFe trilayers. Our numerical simulations confirmed that this frequency dependence stems from the difference between the effective magnetizations of the two magnetic layers. The systematic uncertainties in the experimental determination of the interlayer exchange coupling field caused by this frequency dependence were minimized by fitting broadband experimental FMR data using the full numerical model. A comparison of the comprehensive temperature dependent results with the existing theoretical models, reveals that the thermal spin wave model shows a better agreement with the experimental data.

ACKNOWLEDGMENTS

We would like to acknowledge support by NSF-CAREER Award # 0952929 and by NSF-CAREER Award # 1452670.

Figure Captions:

Figure 1: Schematic diagram showing (a) the acoustic (in phase) and (b) the optic (out of phase) FMR modes in an interlayer exchange coupled trilayer. For the FM(AF) coupling the optic mode has a higher (lower) energy due to the exchange interaction. FM_1 and FM_2 stand for the two ferromagnetic layers and NM represents the non-magnetic spacer layer. $\vec{M}_1$ and $\vec{M}_2$ indicate the magnetization vectors of the two ferromagnetic layers and $\vec{H}_{eff}$ is the effective static magnetic field.

Figure 2: The geometry of the interlayer exchange-coupled structure used for the numerical simulations. The z axis is normal to the thin film structure, while the static magnetic field is applied in the film plane of the trilayer along the x direction.

Figure 3: Simulated Kittel plots based on equation (2) with an assumption of M_{eff} of $1300\ \frac{\text{emu}}{\text{cm}^3}$ and $1400\ \frac{\text{emu}}{\text{cm}^3}$ for a trilayer with 5 nm and 8 nm thick CoFe layers. The exchange field was set to (a) $H_{ex} = -400$ Oe, (b) $H_{ex} = -100$ Oe, (c) $H_{ex} = 0$ Oe, (d) $H_{ex} = 100$ Oe, and (e) $H_{ex} = 400$ Oe. A negative sign corresponds to an antiferromagnetic coupling. The deviations observed in the resonance position of the optic and acoustic modes at low frequencies for the AF coupled samples indicates that the samples are not saturated as the external magnetic field is not large enough to overcome the antiferromagnetic interlayer exchange coupling, see figure 3(a) and its inset.

Figure 4: Simulated frequency dependence of the mode separation $H_{res,ac} - H_{res,op}$ based on equation (2) with an assumption of (a) M_{eff} of $1300\ \frac{\text{emu}}{\text{cm}^3}$ and $1400\ \frac{\text{emu}}{\text{cm}^3}$ for a trilayer with 5 nm and 8 nm $CoFe$ layers thick for different coupling fields. The dashed line represents the

zero coupling case and therefore the two resonances are simply the normal FMR modes of each layer. Part (b) shows that frequency dependence of the mode separation disappears when identical effective magnetizations M_{eff} of $1400\ \frac{\text{emu}}{\text{cm}^3}$ for both $5nm$ and $8nm$ $CoFe$ layers are assumed.

Figure 5: (a),(c) Raw FMR spectra for the $CoFe(5\text{ nm})/Ru(0.8\text{ nm})/CoFe(8\text{ nm})$ and $CoFe(5\text{ nm})/Ru(2\text{ nm})/CoFe(8\text{ nm})$ antiferromagnetically (AF) coupled samples. (b),(d) Raw FMR spectra for the $CoFe(5\text{ nm})/Ru(1.4\text{ nm})/CoFe(8\text{ nm})$ and $CoFe(5\text{ nm})/Ru(2.6\text{ nm})/CoFe(8\text{ nm})$ ferromagnetically (FM) coupled samples. Note that the optic mode appears on the low field side of the acoustic mode for the ferromagnetic coupling and on the high field side for the antiferromagnetic coupling.

Figure 6: (a),(c) Plots of ferromagnetic resonance frequency as a function of resonance field (Kittel Plots) for the $CoFe(5\text{ nm})/Ru(0.8\text{ nm})/CoFe(8\text{ nm})$ and $CoFe(5\ nm)/Ru(2\text{ nm})/CoFe(8\text{ nm})$ antiferromagnetically (AF) coupled samples. (b),(d) Kittel Plots for the $CoFe(5\text{ nm})/Ru(1.4\text{ nm})/CoFe(8\text{ nm})$ and $CoFe(5\text{ nm})/Ru(2.6\text{ nm})/CoFe(8\text{ nm})$ ferromagnetically (FM) coupled samples. The data in black color correspond to the acoustic mode and green corresponds to the optic mode. The symbols represent the experimental data and lines are the fits to the experimental data using the full numerical model, see equation (4).

Figure 7: Frequency dependence of the mode separation $H_{res,ac} - H_{res,op}$ for the $CoFe(5\text{ nm})/Ru(0.8\ nm)/CoFe(8\text{ nm})$ (blue), $CoFe(5\text{ nm})/Ru(2\ nm)/CoFe(8\text{ nm})$ (magenta) antiferromagnetically (AF) coupled samples and $Cofe(5\text{ nm})/Ru(1.4\text{ nm})/CoFe(8\text{ nm})$ (red) and $CoFe(5\text{ nm})/Ru(2.6\text{ nm})/CoFe(8\text{ nm})$ (orange), ferromagnetically

(FM) coupled samples. The symbols represent the experimental data and the lines show the full numerical fit to the experimental data using the full model, see equation (4).

Figure 8: Frequency dependence of the mode separation $H_{res,ac} - H_{res,op}$ for the (a) $CoFe(5\text{ nm})/Ru(0.8\text{ nm})/CoFe(8\text{ nm})$ and (b) $CoFe(5\text{ nm})/Ru(1.4\text{ nm})/CoFe(8\text{ nm})$ samples, as a function of temperature. The symbols represent the experimental data and the lines show the full numerical fit to the experimental data using the full model, see equation (4).

Figure 9: Interlayer exchange coupling field H_{ex} of the $CoFe/Ru(x)/CoFe$ interlayer exchange coupled system as a function of Ru thickness from room temperature down to 10 K. . The $t_{Ru} = 2.2$ nm and $t_{Ru} = 2.4$ nm data correspond to the samples where the optic and acoustic signals were merged together due to a very weak coupling, therefore preventing the determination of the interlayer exchange coupling field, which in these cases was set to zero.

Figure 10: Temperature dependence of the absolute value of the interlayer exchange coupling constant J_{inter} for the $CoFe(5\text{ nm})/Ru(0.8\text{ nm})/CoFe(8\text{ nm})$ and (a),(b) $CoFe(5\text{ nm})/Ru(1.2\text{ nm})/CoFe(8\text{ nm})$ samples (c),(d). The experimental data are represented by symbols, the blue line is a fit to the data using equation (11) with a fixed value of $y = 1.5$, whereas the red line is a fit using equation (9). Both fits are weighted with the standard deviation of the individual data points and confidence bands are shown as shaded areas.

Figure 11: (a) Fit parameter c of the spacer and interface model described by equation (9) as a function of Ru thickness. (b) The fit parameter x of equation (11) as a function of Ru thickness

References:

1. A. Layadi and J. O. Artman, Effect of biquadratic coupling and in-plane anisotropy on the resonance modes of a trilayer system, Journal of Magnetism and Magnetic Materials **92** (1), 143-154 (1990).
2. S. M. Rezende, C. Chesman, M. A. Lucena, A. Azevedo, F. M. de Aguiar and S. S. P. Parkin, Studies of coupled metallic magnetic thin-film trilayers, Journal of Applied Physics **84** (2), 958-972 (1998).
3. Z. Zhang, P. E. Wigen and K. Ounadjela, FMR in strongly coupled Co/Ru/Co structures, IEEE Transactions on Magnetics **29** (6), 2717-2719 (1993).
4. M. D. Stiles, Interlayer exchange coupling, Journal of Magnetism and Magnetic Materials **200** (1–3), 322-337 (1999).
5. P. Bruno, Theory of interlayer magnetic coupling , Physical Review B **52** (1), 411-439 (1995).
6. M. A. Ruderman and C. Kittel, Indirect Exchange Coupling of Nuclear Magnetic Moments by Conduction Electrons, Physical Review **96** (1), 99-102 (1954).
7. P. Bruno, Theory of interlayer exchange interactions in magnetic multilayers, Journal of Physics: Condensed Matter **11** (48), 9403 (1999).
8. P. Grünberg, R. Schreiber, Y. Pang, M. B. Brodsky and H. Sowers, Layered Magnetic Structures: Evidence for Antiferromagnetic Coupling of Fe Layers across Cr Interlayers,Physical Review Letters **57** (19), 2442-2445 (1986).
9. C. F. Majkrzak, J. W. Cable, J. Kwo, M. Hong, D. B. McWhan, Y. Yafet, J. V. Waszczak and C. Vettier, Observation of a Magnetic Antiphase Domain Structure with Long-Range Order in a Synthetic Gd-Y Superlattice, Physical Review Letters **56** (25), 2700-2703 (1986).
10. M. B. Salamon, S. Sinha, J. J. Rhyne, J. E. Cunningham, R. W. Erwin, J. Borchers and C. P. Flynn, Long-range incommensurate magnetic order in a Dy-Y multilayer, Physical Review Letters **56** (3), 259-262 (1986).
11. E. Chen, D. Apalkov, A. Driskill-Smith, A. Khvalkovskiy, D. Lottis, K. Moon, V. Nikitin, A. Ong, X. Tang, S. Watts, R. Kawakami, M. Krounbi, S. A. Wolf, S. J. Poon, J. W. Lu, A. W. Ghosh, M. Stan, W. Butler, T. Mewes, S. Gupta, C. K. A. Mewes, P. B. Visscher and R. A. Lukaszew, Progress and Prospects of Spin Transfer Torque Random Access Memory, IEEE Transactions on Magnetics **48** (11), 3025-3030 (2012).
12. M. N. Baibich, J. M. Broto, A. Fert, F. N. Van Dau, F. Petroff, P. Etienne, G. Creuzet, A. Friederich and J. Chazelas, Giant Magnetoresistance of (001)Fe/(001)Cr Magnetic Superlattices, Physical Review Letters **61** (21), 2472-2475 (1988).
13. Z. Zhang, L. Zhou, P. E. Wigen and K. Ounadjela, Angular dependence of ferromagnetic resonance in exchange-coupled Co/Ru/Co trilayer structures, Physical Review B **50** (9), 6094-6112 (1994).
14. B. Heinrich, Z. Celinski, J. F. Cochran, W. B. Muir, J. Rudd, Q. M. Zhong, A. S. Arrott, K. Myrtle and J. Kirschner, Ferromagnetic and antiferromagnetic exchange coupling in bcc epitaxial ultrathin Fe(001)/Cu(001)Fe(001) trilayers, Physical Review Letters **64** (6), 673-676 (1990).
15. B. Heinrich, S. T. Purcell, J. R. Dutcher, K. B. Urquhart, J. F. Cochran and A. S. Arrott, Structural and magnetic properties of ultrathin Ni/Fe bilayers grown epitaxially on Ag(001), Physical Review B **38** (18), 12879-12896 (1988).
16. A. Layadi, Effect of biquadratic coupling and in-plane anisotropy on the resonance modes of a trilayer system, Physical Review B **65** (10), 104422 (2002).

17. J. Lindner and K. Baberschke, In situ ferromagnetic resonance: an ultimate tool to investigate the coupling in ultrathin magnetic films, Journal of Physics: Condensed Matter **15** (4), R193 (2003).
18. B. Khodadadi, Investigation of magnetic relaxation mechanisms and dynamic magnetic properties in thin films using ferromagnetic resonance (FMR) technique, in *Department of Physics and Astronomy* ,The University of Alabama, Doctor of Philosophy Thesis, (2016).
19. Y. Cui, B. Khodadadi, S. Schäfer, T. Mewes, J. Lu and S. A. Wolf, Interfacial perpendicular magnetic anisotropy and damping parameter in ultra thin Co2FeAl films, Applied Physics Letters **102** (16), 162403 (2013).
20. S. Keshavarz, Y. Xu, S. Hrdy, C. Lemley, T. Mewes and Y. Bao, Relaxation of Polymer Coated Magnetic Nanoparticles in Aqueous Solution, IEEE Transactions on Magnetics **46** (6), 1541-1543 (2010).
21. S. Klingler, A V. Chumak, T. Mewes, B. Khodadadi, C. Mewes, C. Dubs, O. Surzhenko, B. Hillebrands and A. Conca, Measurements of the exchange stiffness of YIG films using broadband ferromagnetic resonance techniques, Journal of Physics D: Applied Physics **48** (1), 015001 (2015).
22. C. Sterwerf, S. Paul, B. Khodadadi, M. Meinert, J.-M. Schmalhorst, M. Buchmeier, C. K. A. Mewes, T. Mewes and G. Reiss, Low Gilbert damping in Co2FeSi and Fe2CoSi films, Journal of Applied Physics **120** (8), 083904 (2016).
23. N. Pachauri, B. Khodadadi, A. V. Singh, J. B. Mohammadi, R. L. Martens, P. R. LeClair, C. Mewes, T. Mewes and A. Gupta, A comprehensive study of ferromagnetic resonance and structural properties of iron-rich nickel ferrite (NixFe3−xO4, x≤1) films grown by chemical vapor deposition, Journal of Magnetism and Magnetic Materials **417**, 137-142 (2016).
24. Z. Zhang, L. Zhou, P. E. Wigen and K. Ounadjela, Using Ferromagnetic Resonance as a Sensitive Method to Study Temperature Dependence of Interlayer Exchange Coupling, Physical Review Letters **73** (2), 336-339 (1994).
25. B. Heinrich, Spin Relaxation in Magnetic Metallic Layers and Multilayers, in *Ultrathin Magnetic Structures III: Fundamentals of Nanomagnetism*, edited by J. A. C. Bland and B. Heinrich (Springer Berlin Heidelberg, Berlin, Heidelberg, 2005), pp. 143-210.
26. S. Schwieger, J. Kienert, K. Lenz, J. Lindner, K. Baberschke and W. Nolting, Spin-Wave Excitations: The Main Source of the Temperature Dependence of Interlayer Exchange Coupling in Nanostructures, Physical Review Letters **98** (5), 057205 (2007).
27. S. Schwieger and W. Nolting, Origin of the temperature dependence of interlayer exchange coupling in metallic trilayers, Physical Review B **69** (22), 224413 (2004).
28. S. S. Kalarickal, X. Y. Xu, K. Lenz, Dominant role of thermal magnon excitation in temperature dependence of interlayer exchange coupling: Experimental verification, W. Kuch and K. Baberschke, Physical Review B **75** (22), 224429 (2007).
29. J. Lindner, C. Rüdt, E. Kosubek, P. Poulopoulos, K. Baberschke, P. Blomquist, R. Wäppling and D. L. Mills, $T^{3/2}$ Dependence of the Interlayer Exchange Coupling in Ferromagnetic Multilayers, Physical Review Letters **88** (16), 167206 (2002).
30. P. Bruno and C. Chappert, Oscillatory coupling between ferromagnetic layers separated by a nonmagnetic metal spacer, Physical Review Letters **67** (12), 1602-1605 (1991).
31. D. M. Edwards, J. Mathon, R. B. Muniz and M. S. Phan, Oscillations of the exchange in magnetic multilayers as an analog of de Haas–van Alphen effect, Physical Review Letters **67** (4), 493-496 (1991).
32. V. Drchal, J. Kudrnovský, P. Bruno, I. Turek, P. H. Dederichs and P. Weinberger, Temperature dependence of the interlayer exchange coupling in magnetic multilayers: An ab initio approach, Physical Review B **60** (13), 9588-9595 (1999).
33. K. Baberschke, Magnetic anisotropy energy and interlayer exchange coupling in ultrathin ferromagnets: Experiment versus theory, Philosophical Magazine **88** (18-20), 2643-2654 (2008).
34. P. Richter, Estimating errors in least-squares fitting, TDA progress report (42), 107 (1995).
35. S. S. P. Parkin, N. More and K. P. Roche, Oscillations in exchange coupling and magnetoresistance in metallic superlattice structures: Co/Ru, Co/Cr, and Fe/Cr, Physical Review Letters **64** (19), 2304-2307 (1990).

36. C. H. Shang, T. P. Weihs, R. C. Cammarata, Y. Ji and C. L. Chien, Anisotropy in magnetic and mechanical properties in textured Hiperco® FeCoV alloys, Journal of Applied Physics **87** (9), 6508-6510 (2000).
37. C.-H. Shang, R. C. Cammarata, T. P. Weihs and C. L. Chien, Microstructure and Hall–Petch Behavior of Fe–Co-based Hiperco© Alloys, Journal of Materials Research **15** (4), 835-837 (2011).

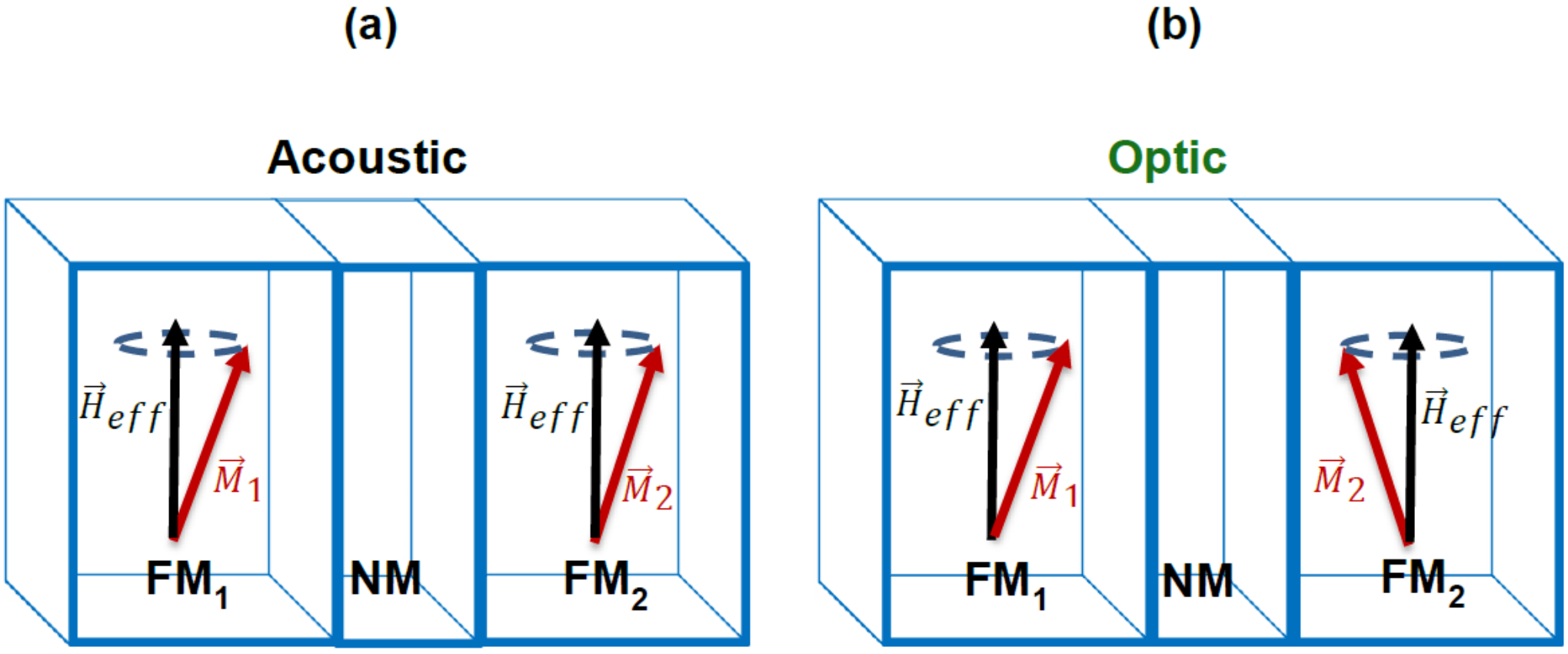
(a)
Acoustic
$\vec{H}_{eff}$
$\vec{M}_1$
$\vec{H}_{eff}$
$\vec{M}_2$
FM1
NM
FM2
(b)
Optic
$\vec{H}_{eff}$
$\vec{M}_1$
$\vec{M}_2$
$\vec{H}_{eff}$
FM1
NM
FM2

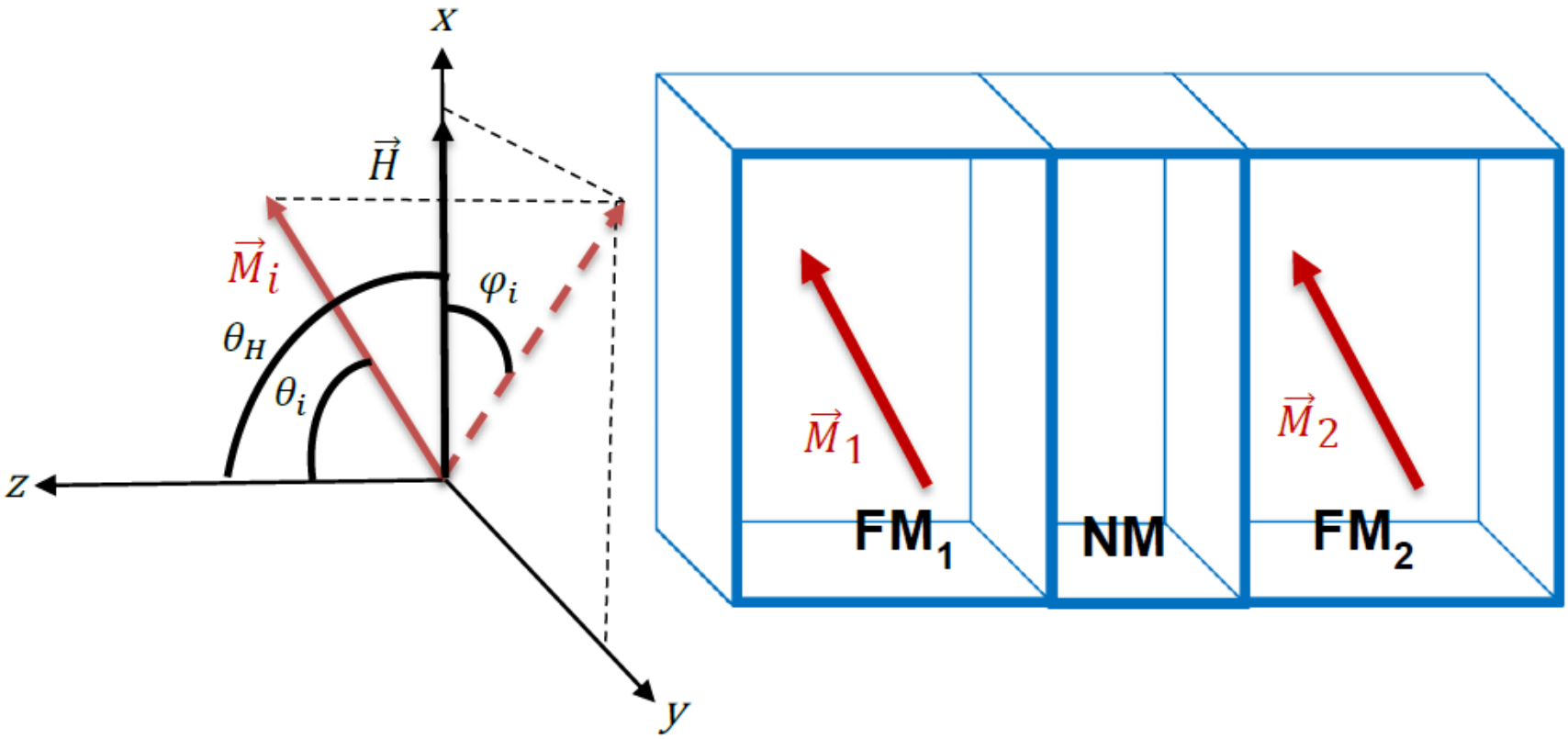
x
$\vec{H}$
$\vec{M}_i$
φ_i
θ_H
θ_i
z
y
$\vec{M}_1$
$\vec{M}_2$
FM1
NM
FM2

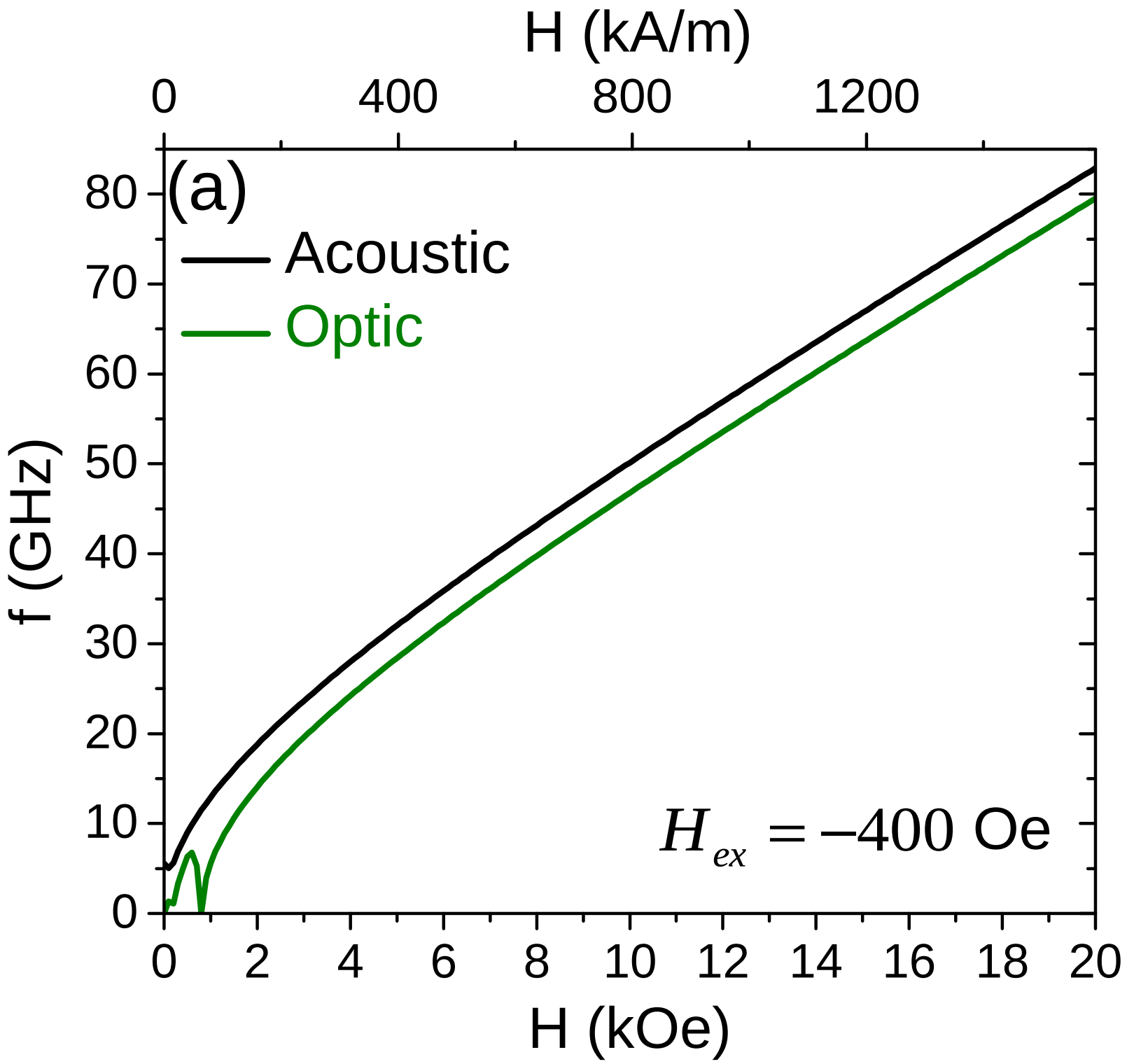
H (kA/m)
0
400
800
1200
(a)
Acoustic
Optic
f (GHz)
80
70
60
50
40
30
20
10
0
$H_{ex} = -400$ Oe
0
2
4
6
8
10
12
14
16
18
20
H (kOe)

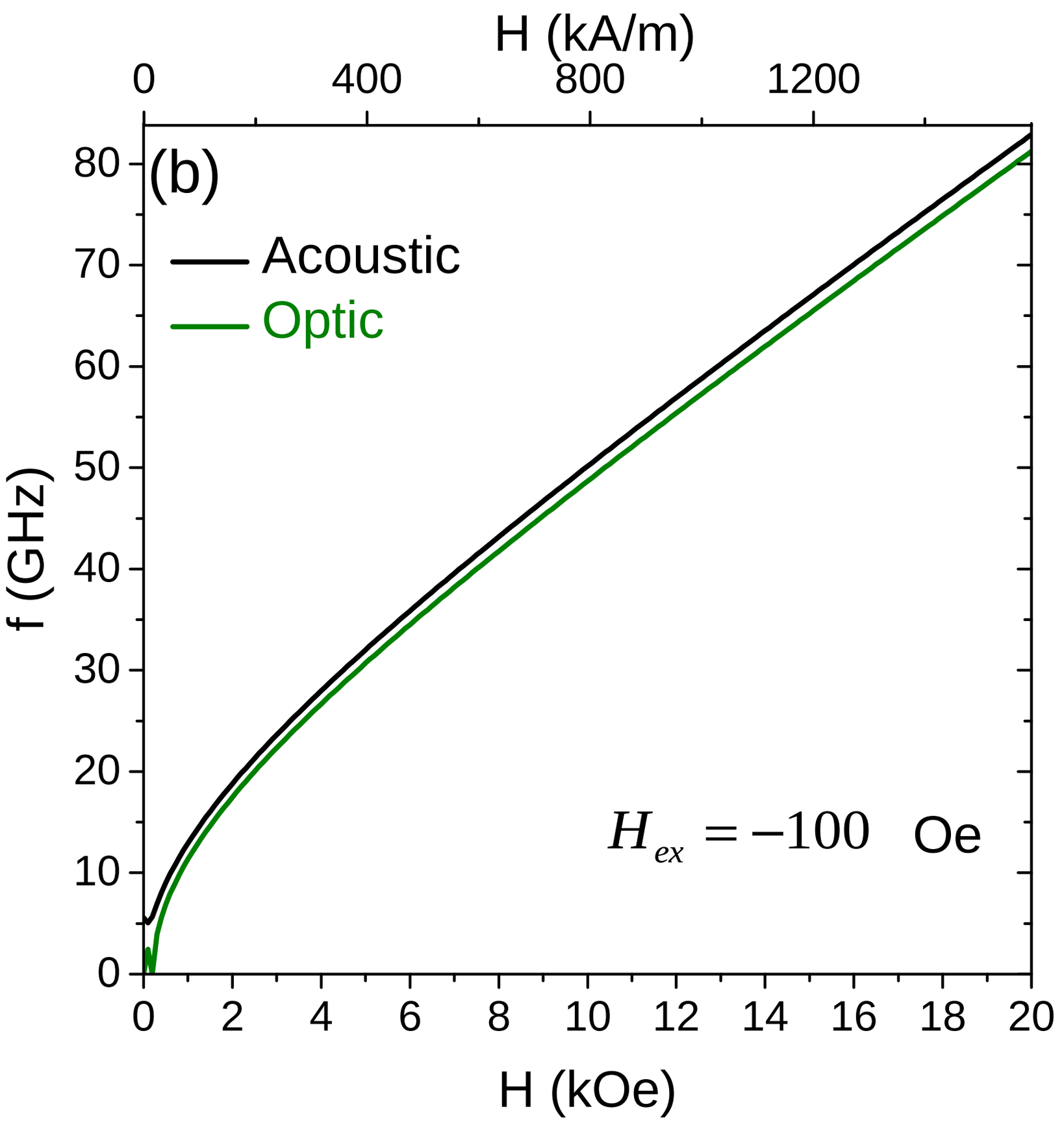
H (kA/m)
0
400
800
1200
(b)
Acoustic
Optic
f (GHz)
80
70
60
50
40
30
20
10
0
$H_{ex} = -100$ Oe
0
2
4
6
8
10
12
14
16
18
20
H (kOe)

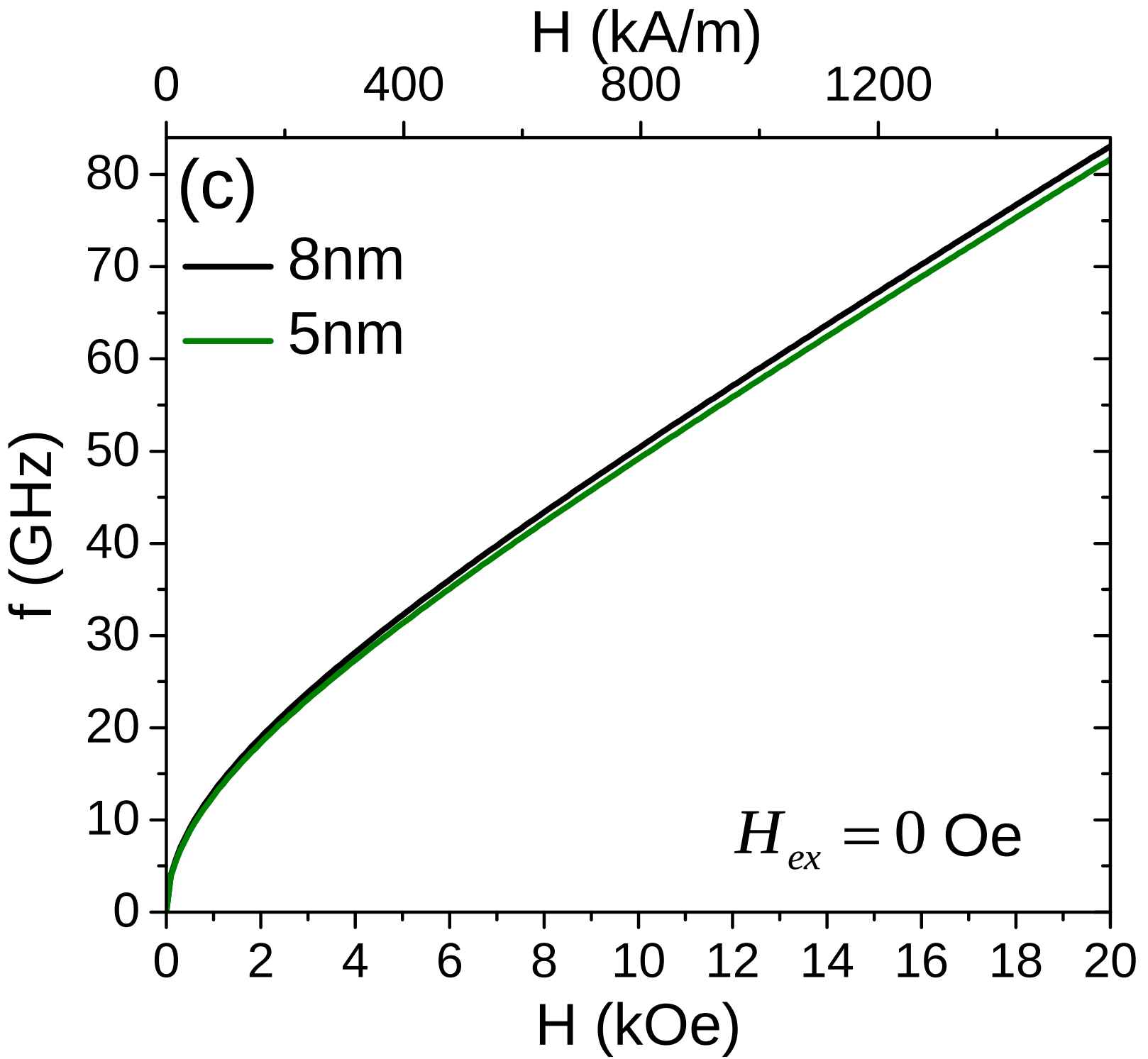
H (kA/m)
0
400
800
1200
(c)
8nm
5nm
f (GHz)
80
70
60
50
40
30
20
10
0
$H_{ex} = 0$ Oe
0
2
4
6
8
10
12
14
16
18
20
H (kOe)

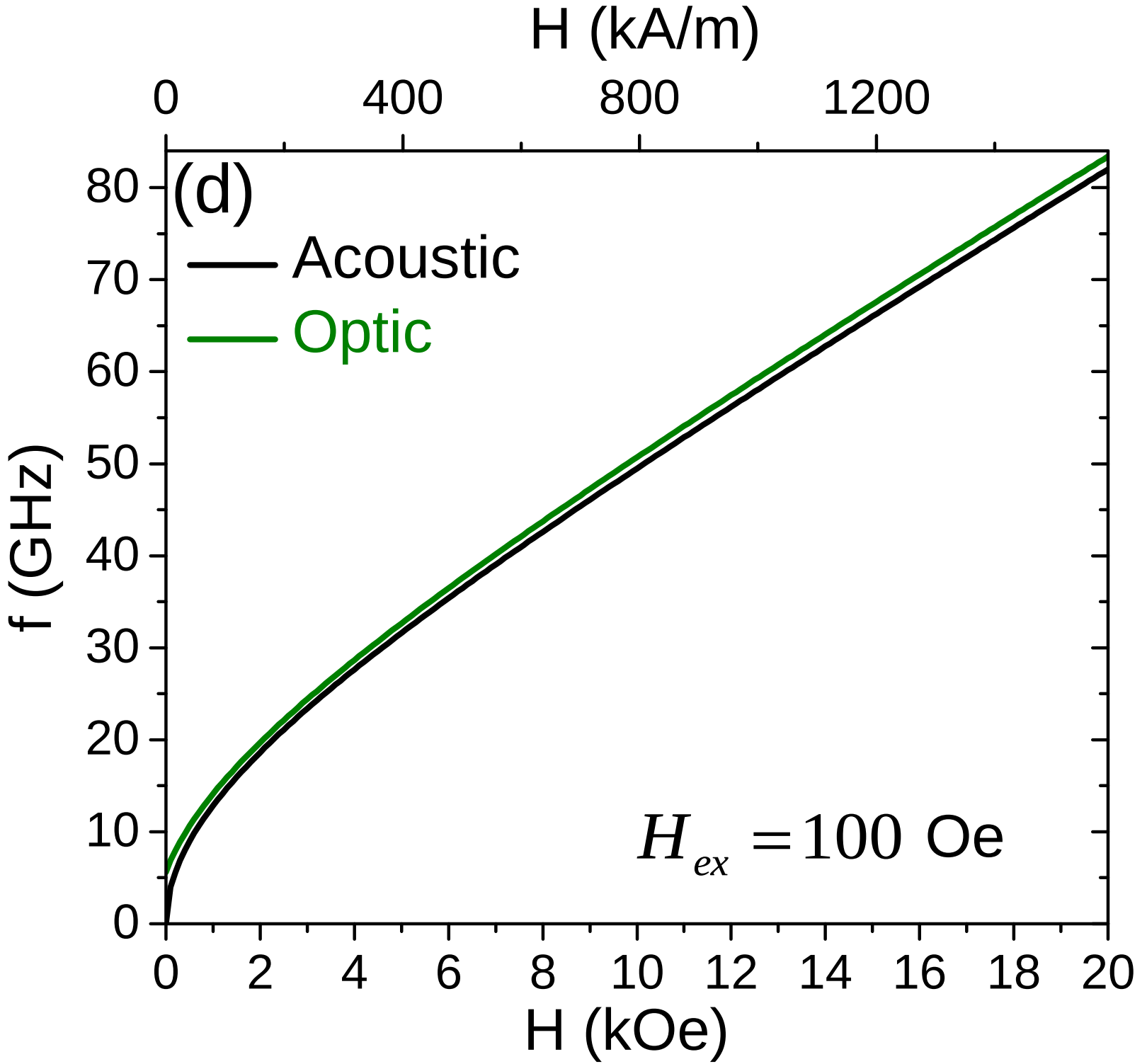
H (kA/m)
0
400
800
1200
(d)
Acoustic
Optic
f (GHz)
80
70
60
50
40
30
20
10
0
$H_{ex} = 100$ Oe
0
2
4
6
8
10
12
14
16
18
20
H (kOe)

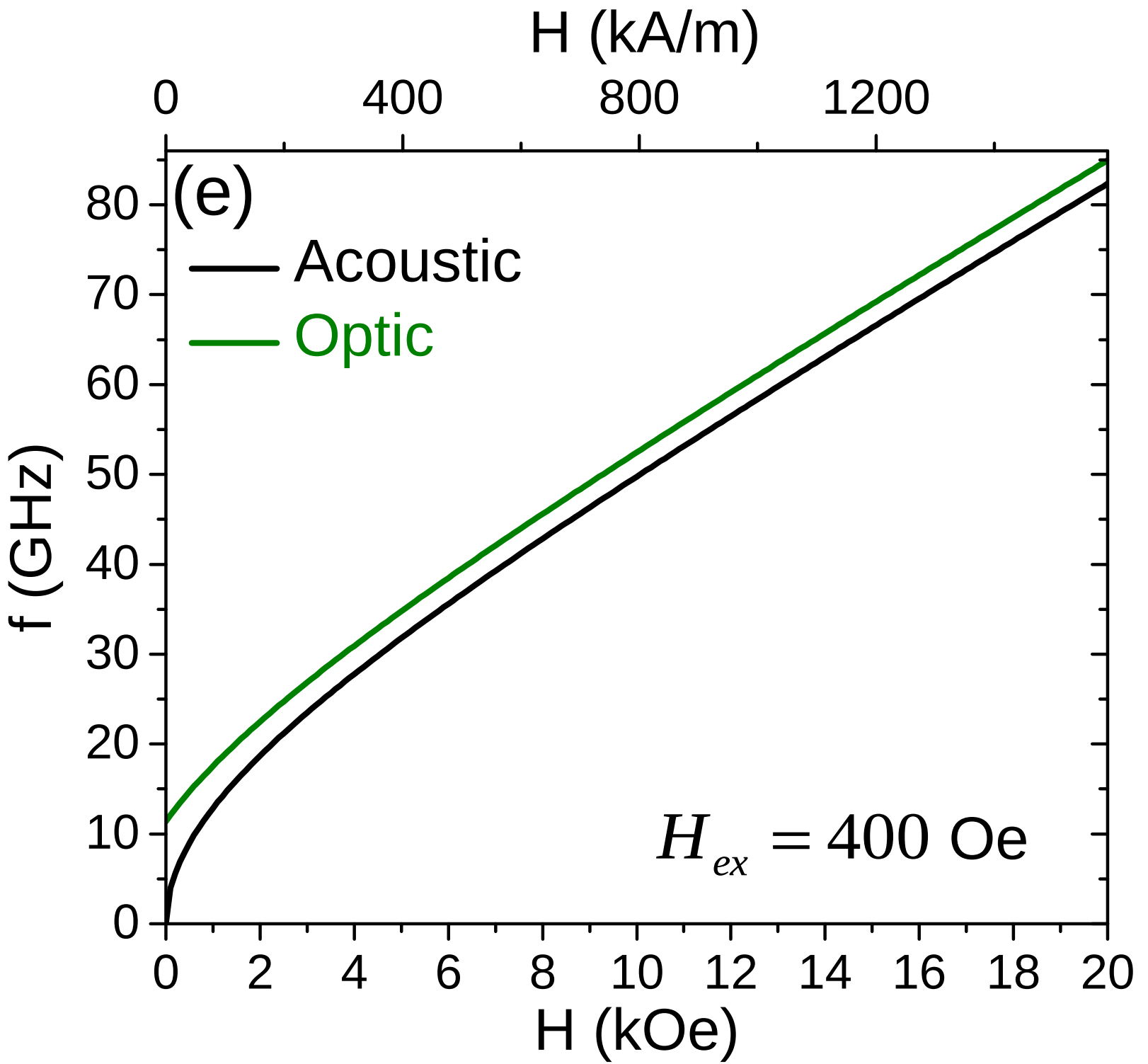
H (kA/m)
0
400
800
1200
(e)
Acoustic
Optic
f (GHz)
0
10
20
30
40
50
60
70
80
$H_{ex} = 400$ Oe
0
2
4
6
8
10
12
14
16
18
20
H (kOe)

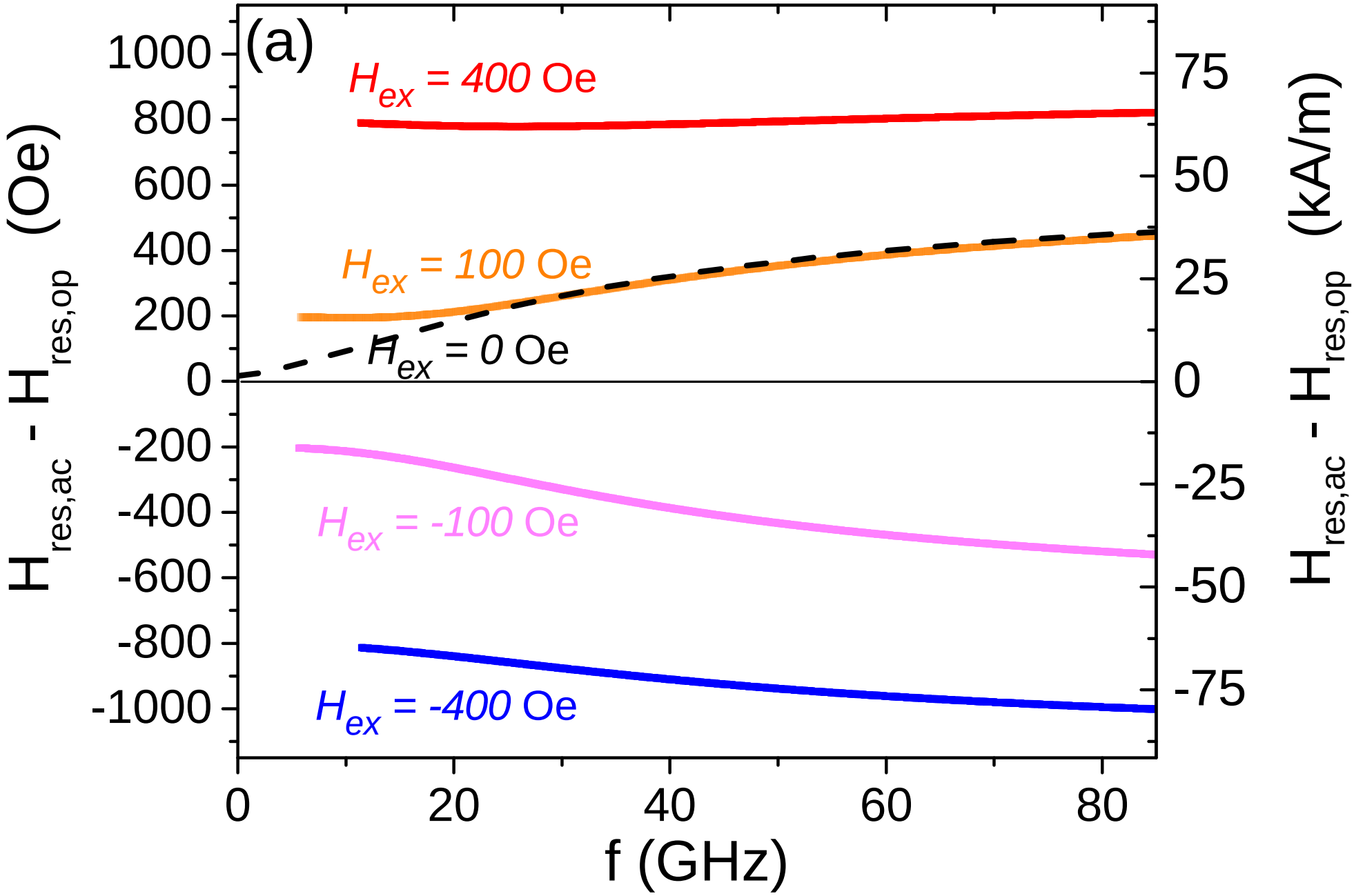
(a)
H_{ex} = 400 Oe
H_{ex} = 100 Oe
H_{ex} = 0 Oe
H_{ex} = -100 Oe
H_{ex} = -400 Oe
1000
800
600
400
200
0
-200
-400
-600
-800
-1000
75
50
25
0
-25
-50
-75
0
20
40
60
80
f (GHz)
$H_{res,ac}$ - $H_{res,op}$ (Oe)
$H_{res,ac}$ - $H_{res,op}$ (kA/m)

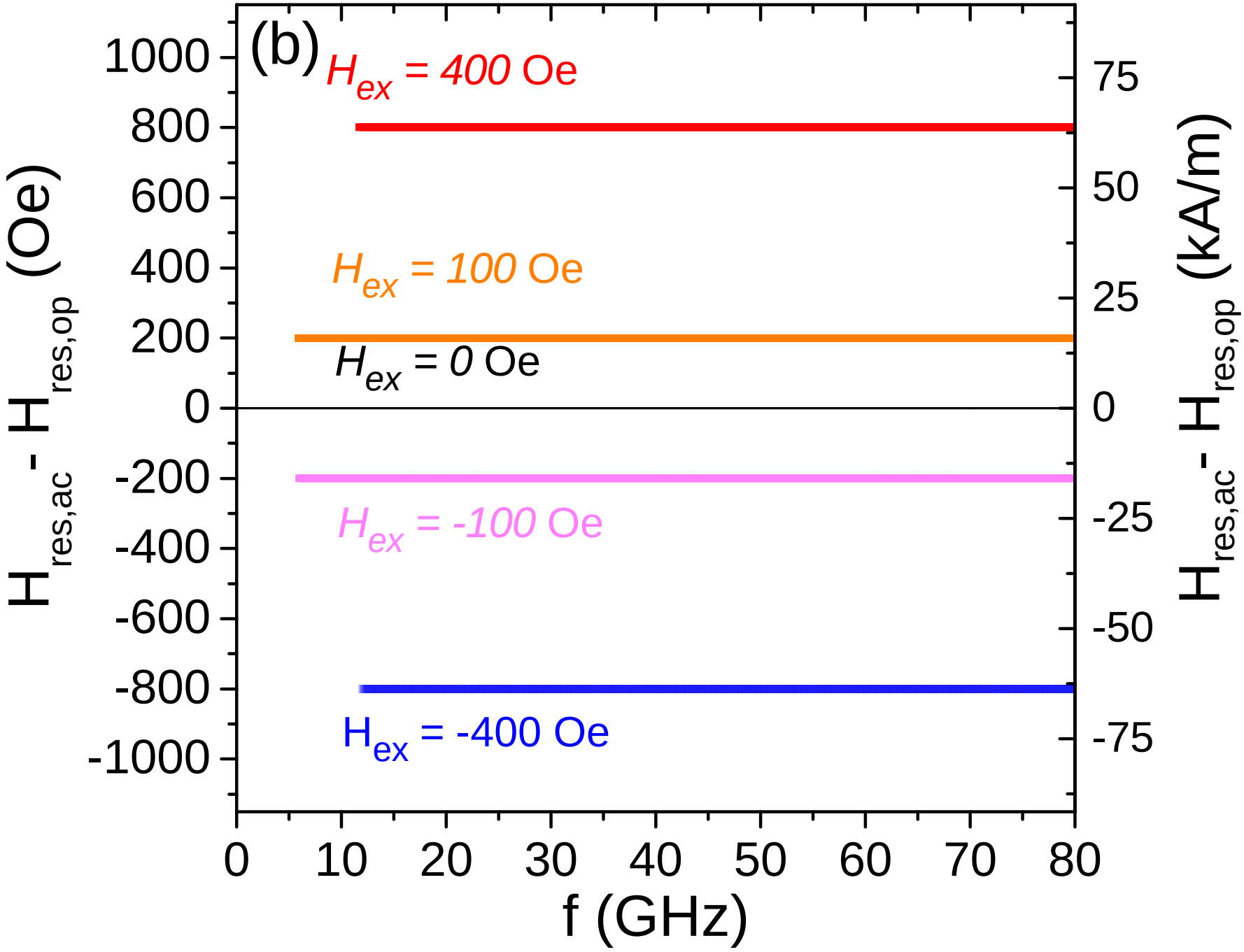
(b)
H_{ex} = 400 Oe
H_{ex} = 100 Oe
H_{ex} = 0 Oe
H_{ex} = -100 Oe
H_{ex} = -400 Oe
1000
800
600
400
200
0
-200
-400
-600
-800
-1000
75
50
25
0
-25
-50
-75
0
10
20
30
40
50
60
70
80
f (GHz)
$H_{res,ac}$ - $H_{res,op}$ (Oe)
$H_{res,ac}$ - $H_{res,op}$ (kA/m)

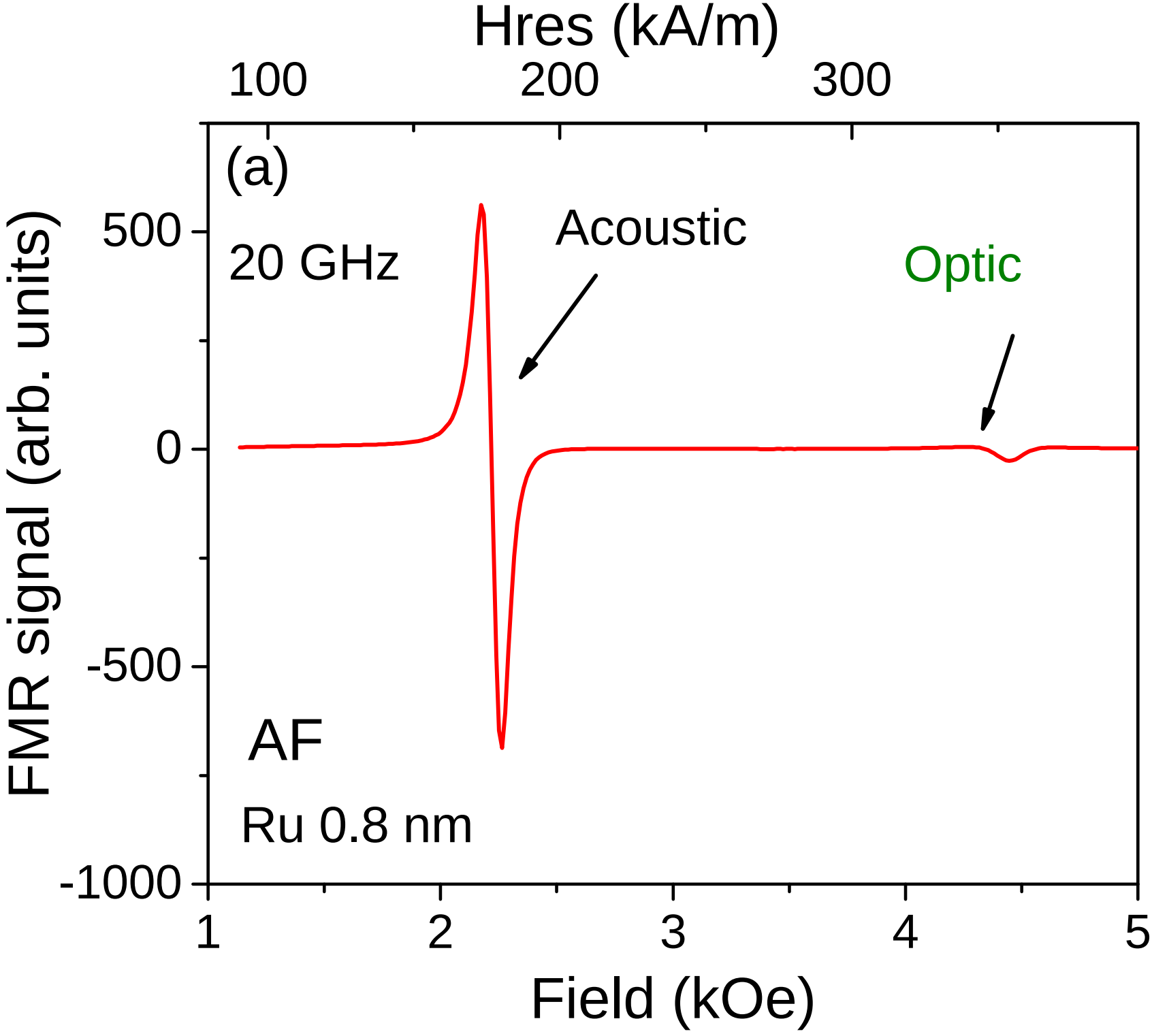
Hres (kA/m)
100
200
300
(a)
20 GHz
Acoustic
Optic
AF
Ru 0.8 nm
FMR signal (arb. units)
500
0
-500
-1000
1
2
3
4
5
Field (kOe)

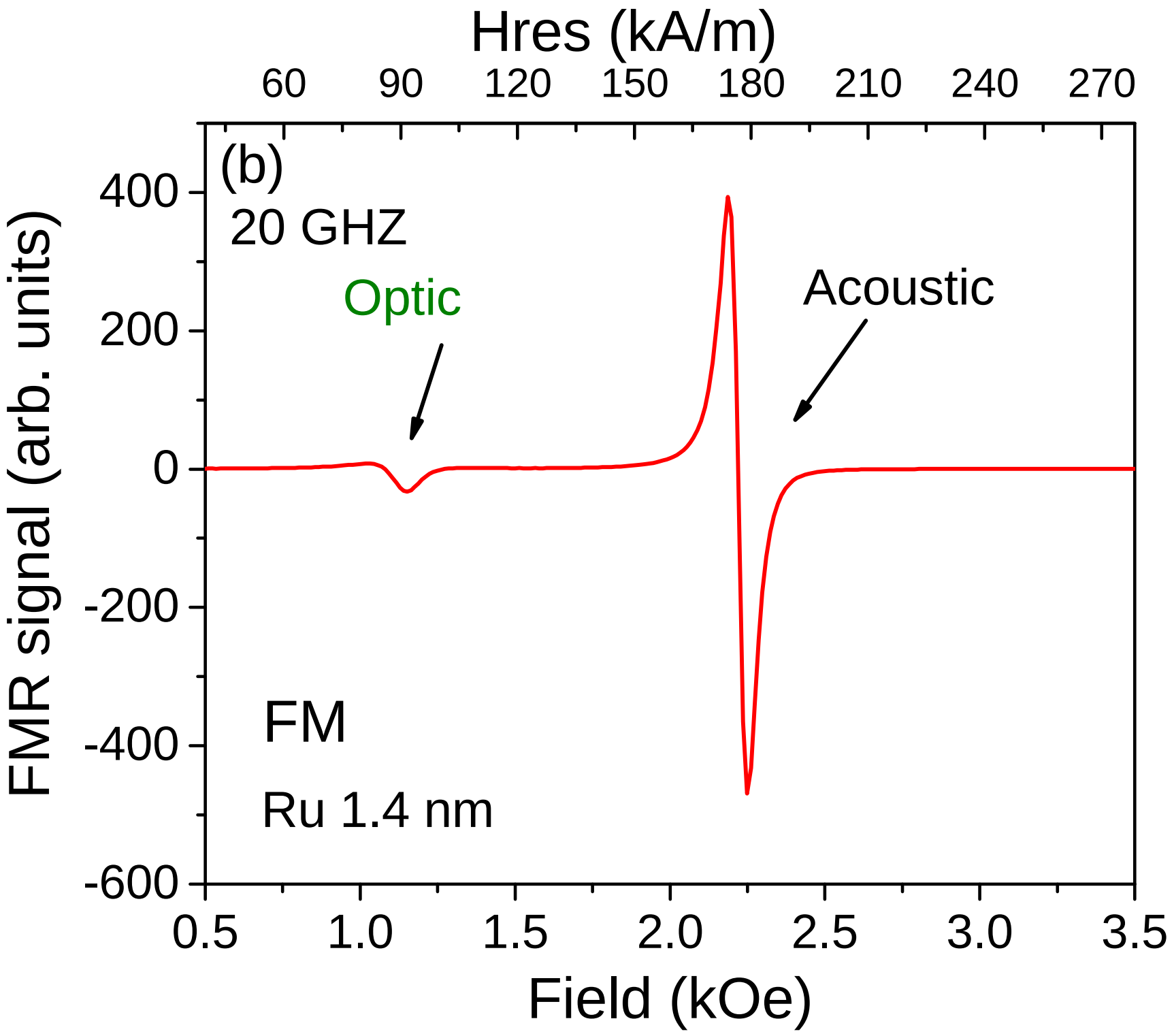
Hres (kA/m)
60
90
120
150
180
210
240
270
(b)
20 GHZ
Optic
Acoustic
FM
Ru 1.4 nm
FMR signal (arb. units)
400
200
0
-200
-400
-600
0.5
1.0
1.5
2.0
2.5
3.0
3.5
Field (kOe)

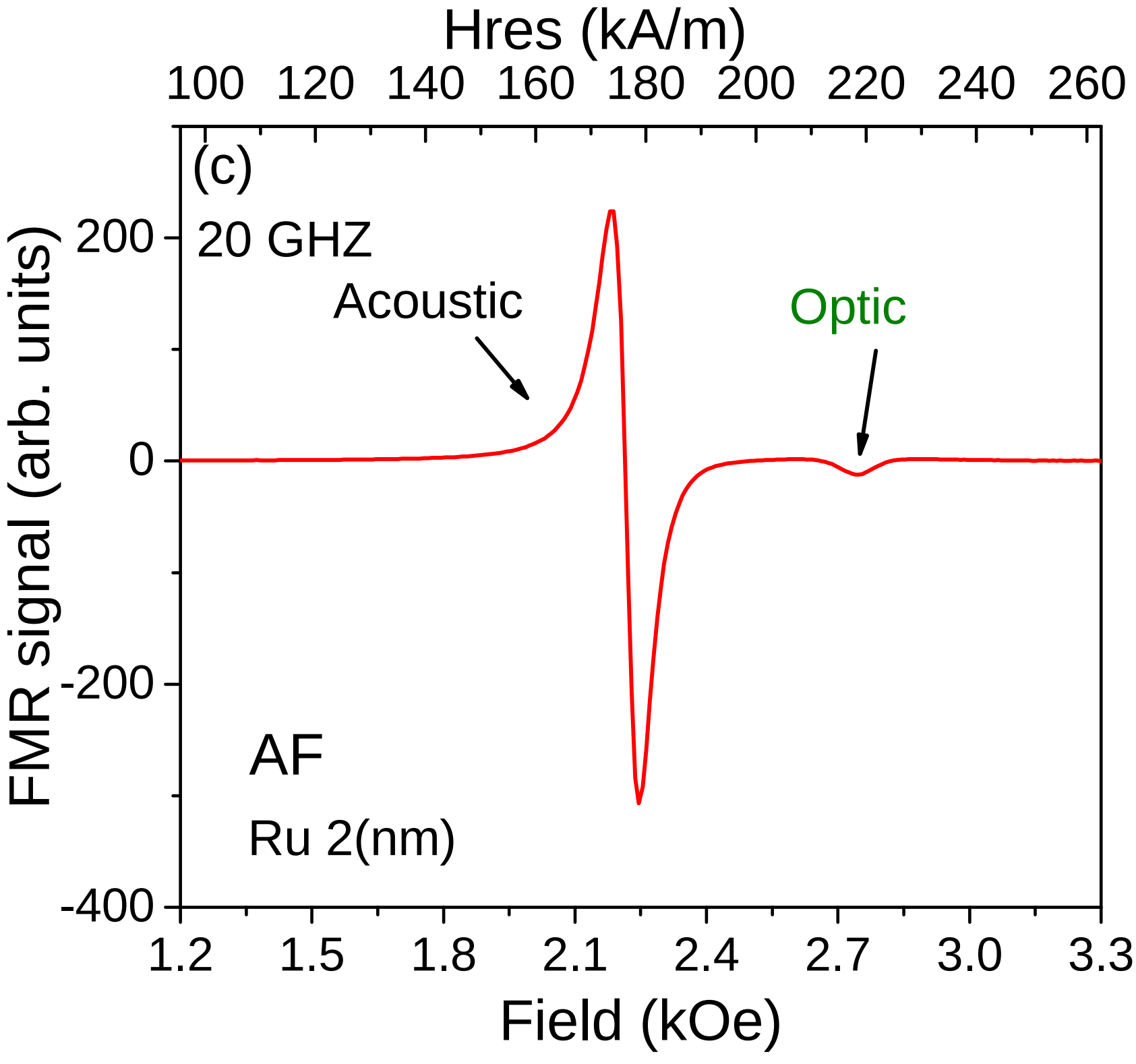
Hres (kA/m)
100 120 140 160 180 200 220 240 260
(c)
20 GHZ
Acoustic
Optic
200
0
-200
-400
AF
Ru 2(nm)
FMR signal (arb. units)
1.2 1.5 1.8 2.1 2.4 2.7 3.0 3.3
Field (kOe)

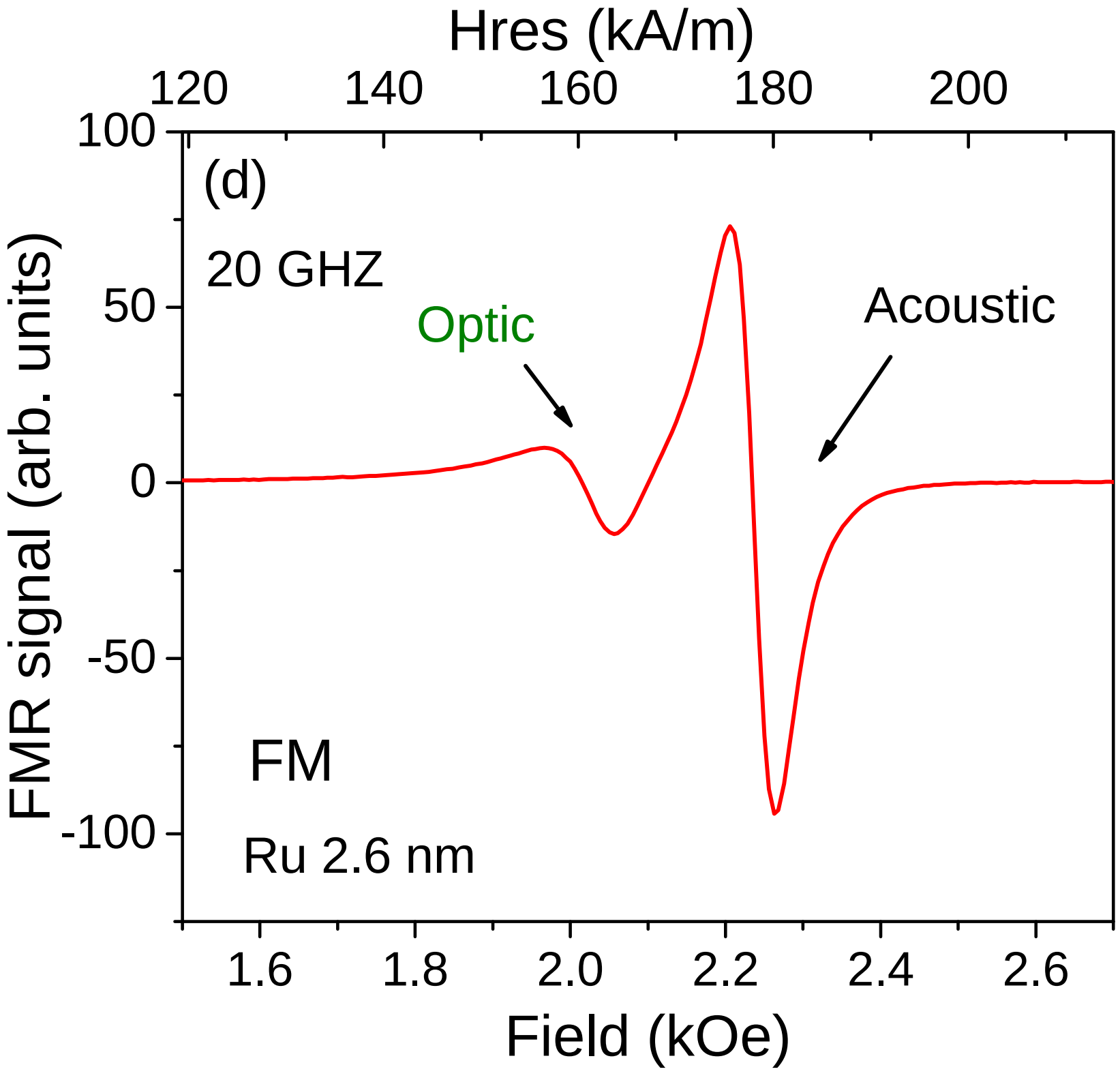
Hres (kA/m)
120
140
160
180
200
100
50
0
-50
-100
(d)
20 GHZ
Optic
Acoustic
FM
Ru 2.6 nm
FMR signal (arb. units)
1.6
1.8
2.0
2.2
2.4
2.6
Field (kOe)

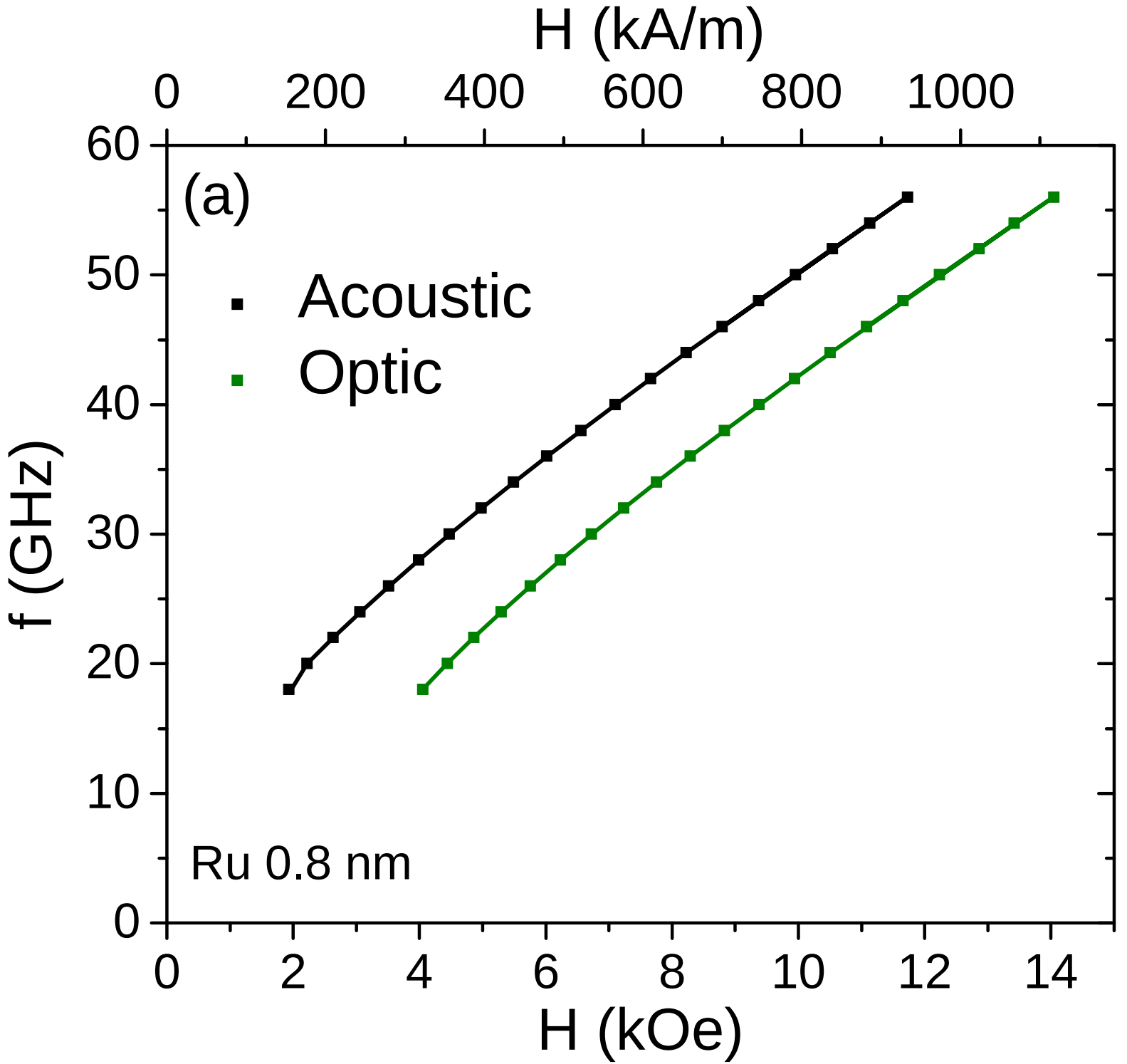
H (kA/m)
0
200
400
600
800
1000
60
50
40
30
20
10
0
(a)
Acoustic
Optic
f (GHz)
Ru 0.8 nm
0
2
4
6
8
10
12
14
H (kOe)

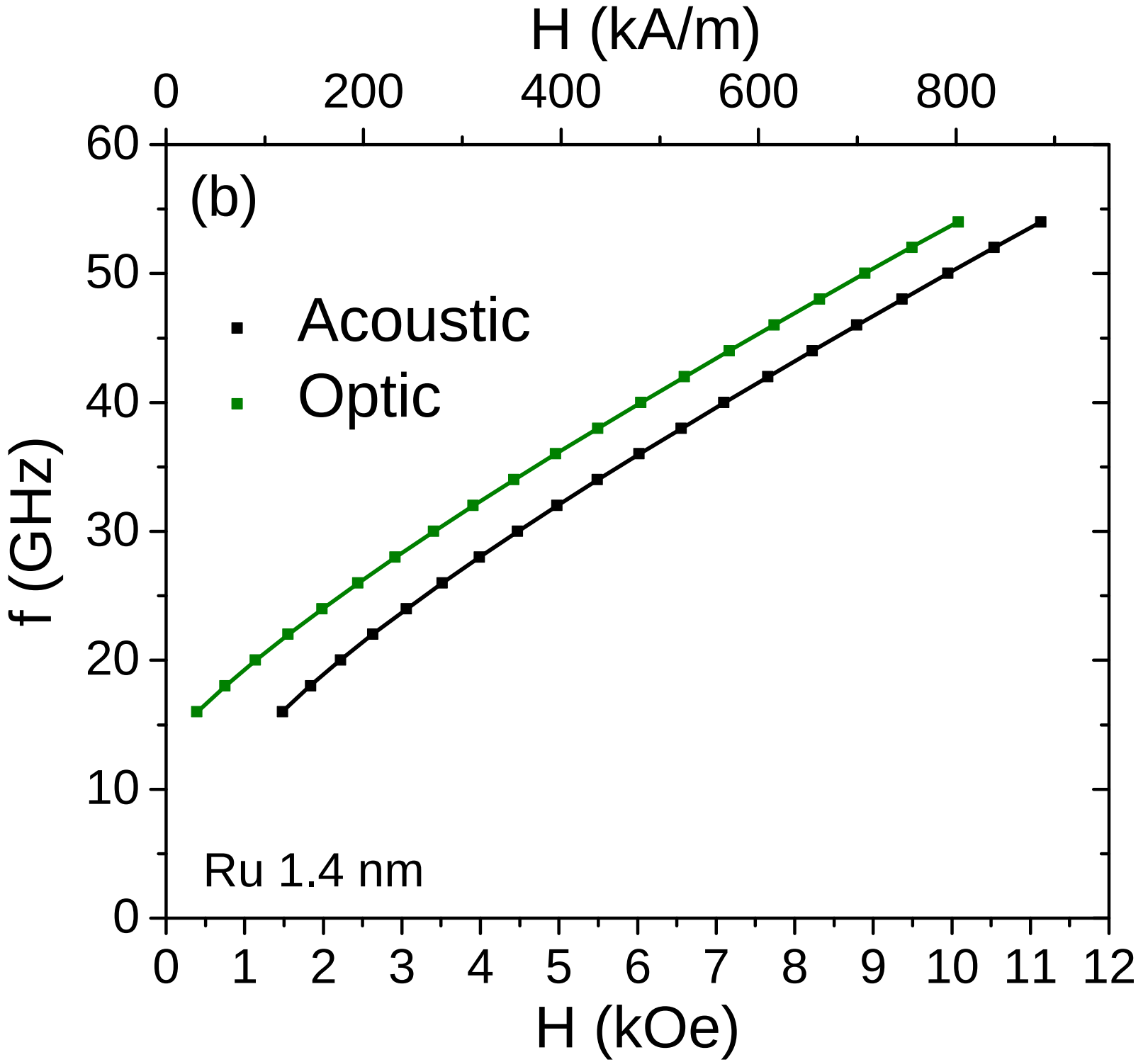
H (kA/m)
0
200
400
600
800
60
50
40
30
20
10
0
(b)
Acoustic
Optic
f (GHz)
Ru 1.4 nm
0
1
2
3
4
5
6
7
8
9
10
11
12
H (kOe)

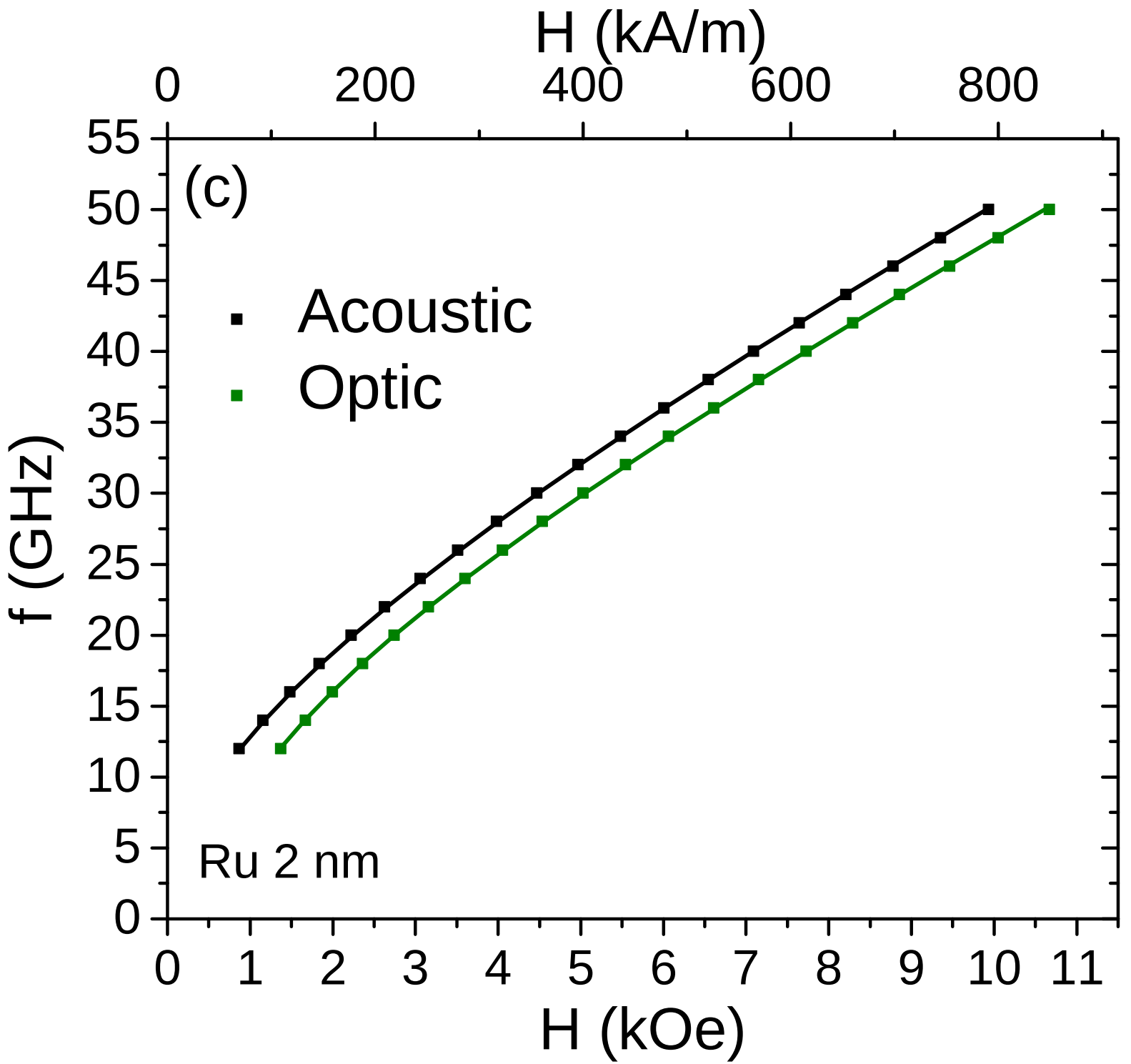
H (kA/m)
0
200
400
600
800
(c)
Acoustic
Optic
Ru 2 nm
f (GHz)
55
50
45
40
35
30
25
20
15
10
5
0
0
1
2
3
4
5
6
7
8
9
10
11
H (kOe)

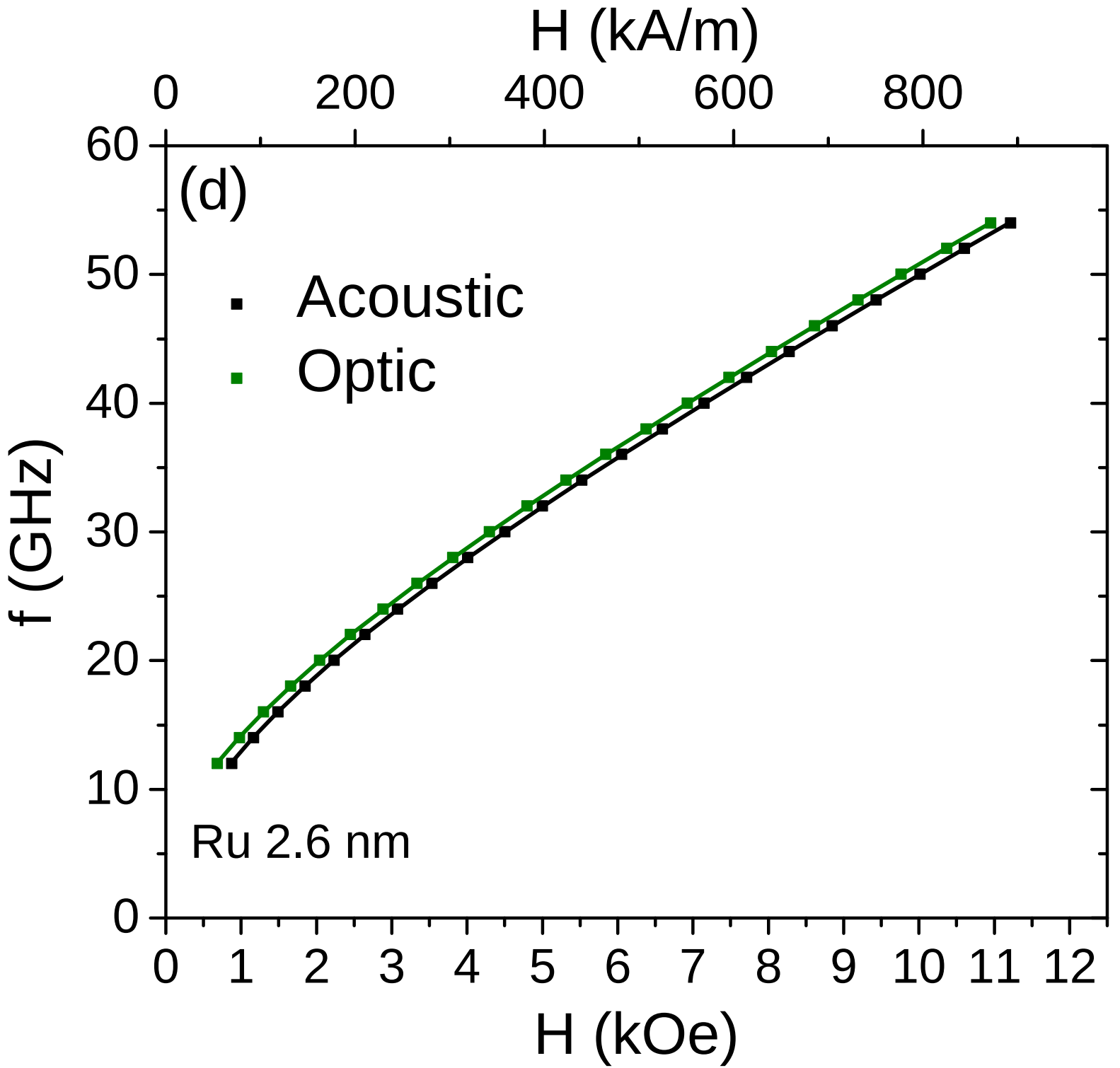
H (kA/m)
0
200
400
600
800
(d)
Acoustic
Optic
f (GHz)
60
50
40
30
20
10
0
Ru 2.6 nm
0
1
2
3
4
5
6
7
8
9
10
11
12
H (kOe)

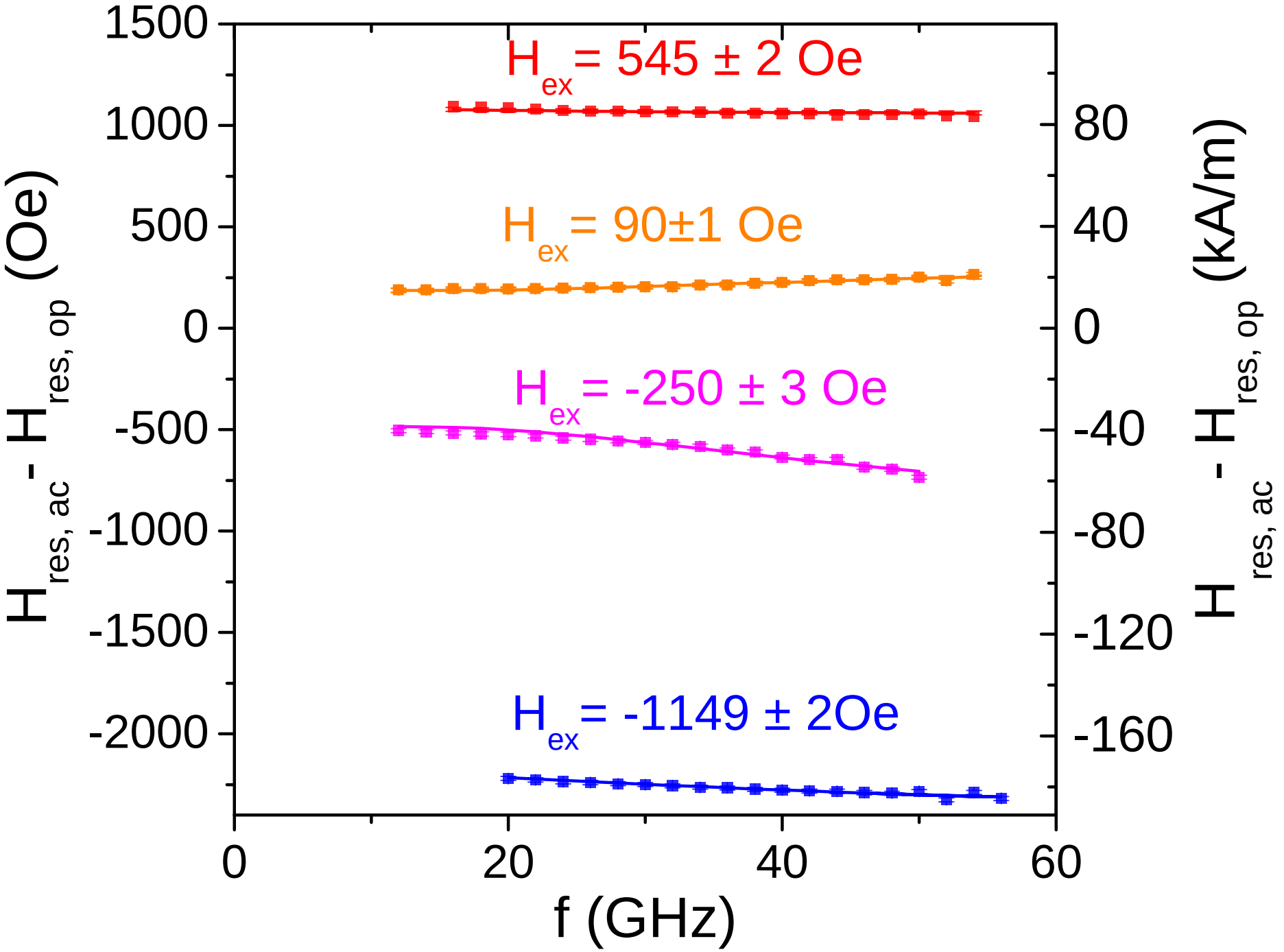
H_ex = 545 ± 2 Oe
H_ex = 90±1 Oe
H_ex = -250 ± 3 Oe
H_ex = -1149 ± 2Oe
H_res, ac - H_res, op (Oe)
H_res, ac - H_res, op (kA/m)
f (GHz)
1500
1000
500
0
-500
-1000
-1500
-2000
80
40
0
-40
-80
-120
-160
0
20
40
60

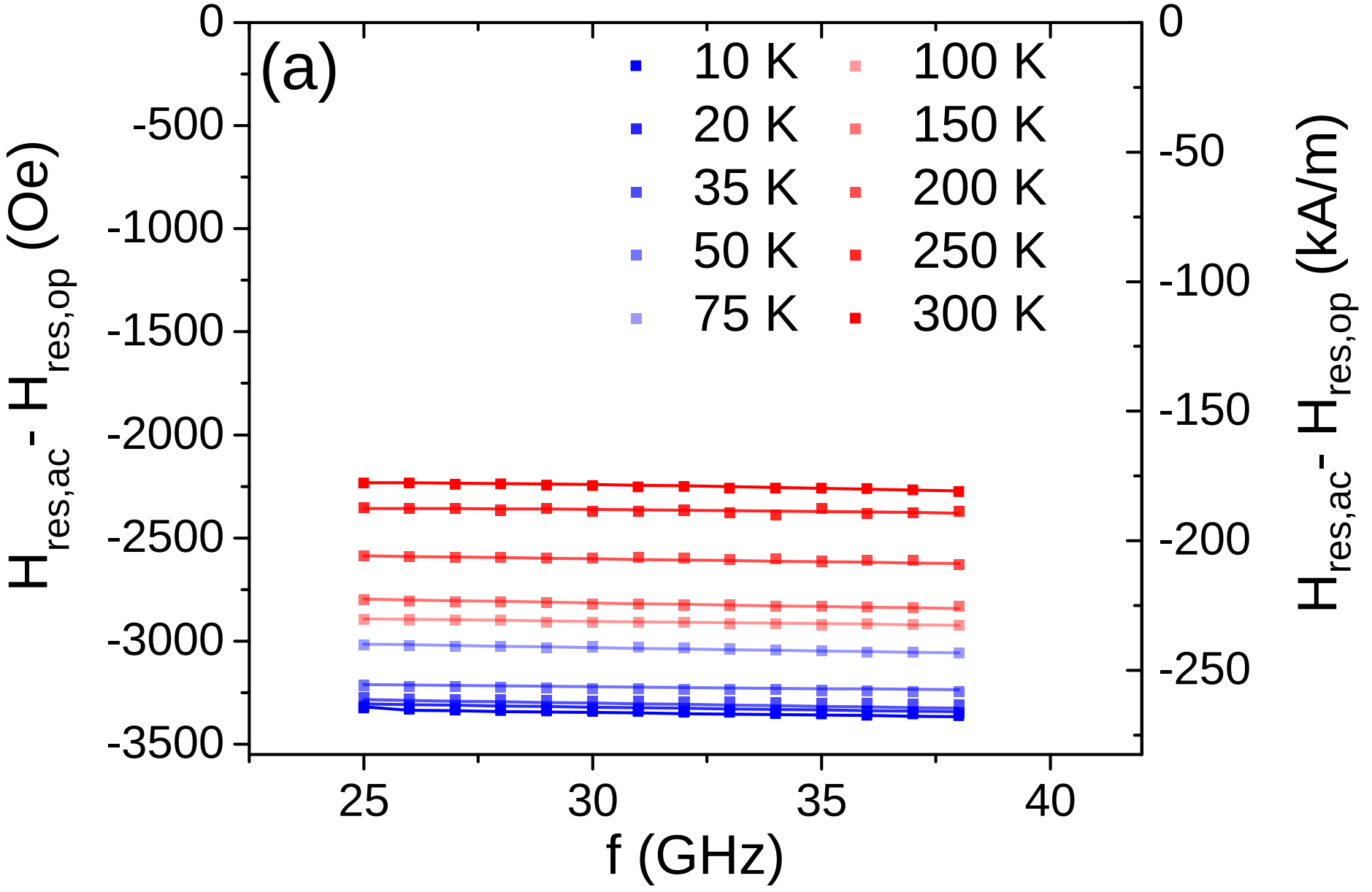
(a)
10 K
20 K
35 K
50 K
75 K
100 K
150 K
200 K
250 K
300 K
0
-500
-1000
-1500
-2000
-2500
-3000
-3500
25
30
35
40
f (GHz)
H_res,ac - H_res,op (Oe)
0
-50
-100
-150
-200
-250
H_res,ac - H_res,op (kA/m)

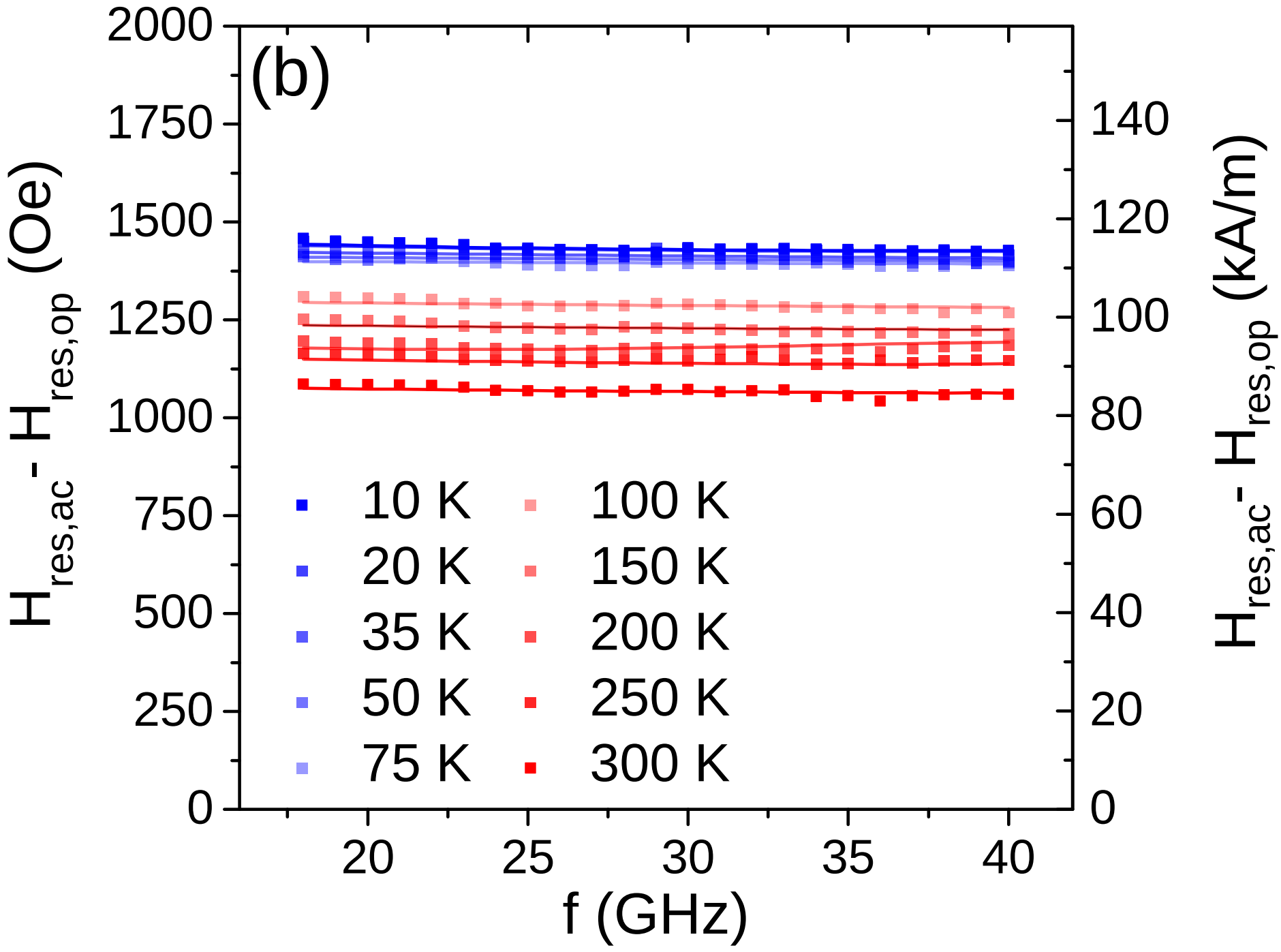
(b)
2000
1750
1500
1250
1000
750
500
250
0
140
120
100
80
60
40
20
0
20
25
30
35
40
f (GHz)
H_res,ac - H_res,op (Oe)
H_res,ac - H_res,op (kA/m)
10 K
20 K
35 K
50 K
75 K
100 K
150 K
200 K
250 K
300 K

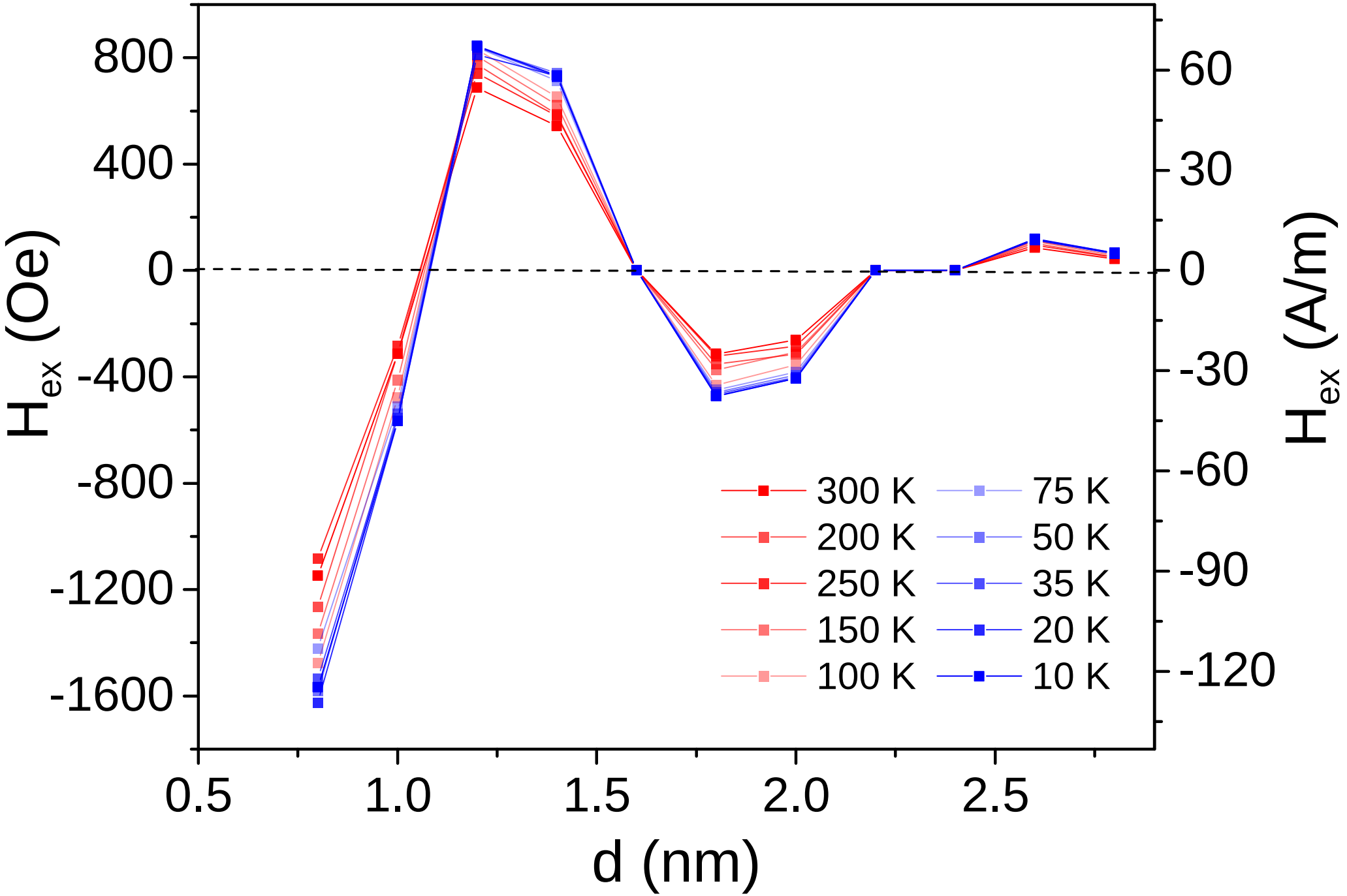
800
400
0
-400
-800
-1200
-1600
H_ex (Oe)
60
30
0
-30
-60
-90
-120
H_ex (A/m)
0.5
1.0
1.5
2.0
2.5
d (nm)
300 K
200 K
250 K
150 K
100 K
75 K
50 K
35 K
20 K
10 K

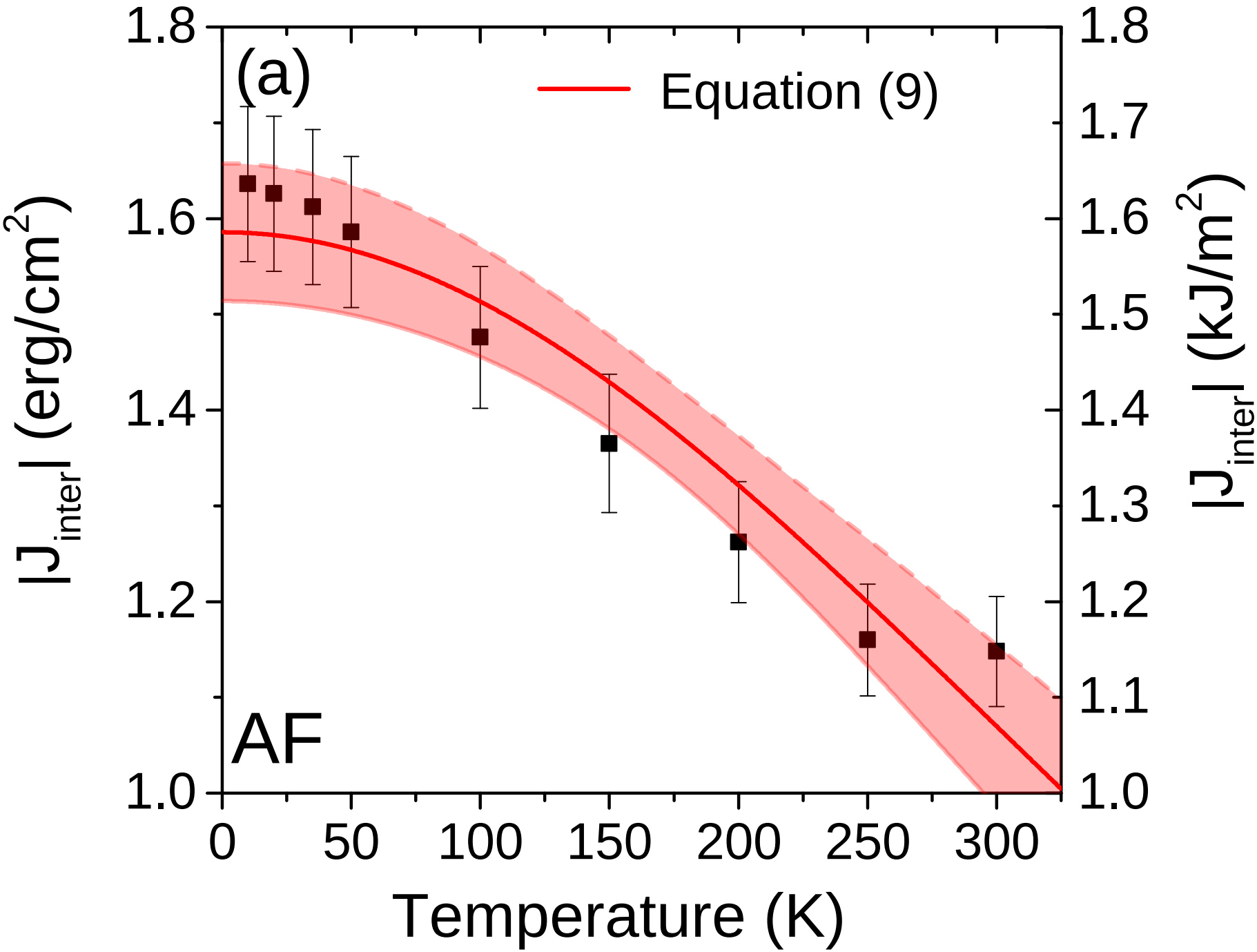
(a)
Equation (9)
AF
1.8
1.6
1.4
1.2
1.0
0
50
100
150
200
250
300
Temperature (K)
|J_inter| (erg/cm^2)
|J_inter| (kJ/m^2)
1.8
1.7
1.6
1.5
1.4
1.3
1.2
1.1
1.0

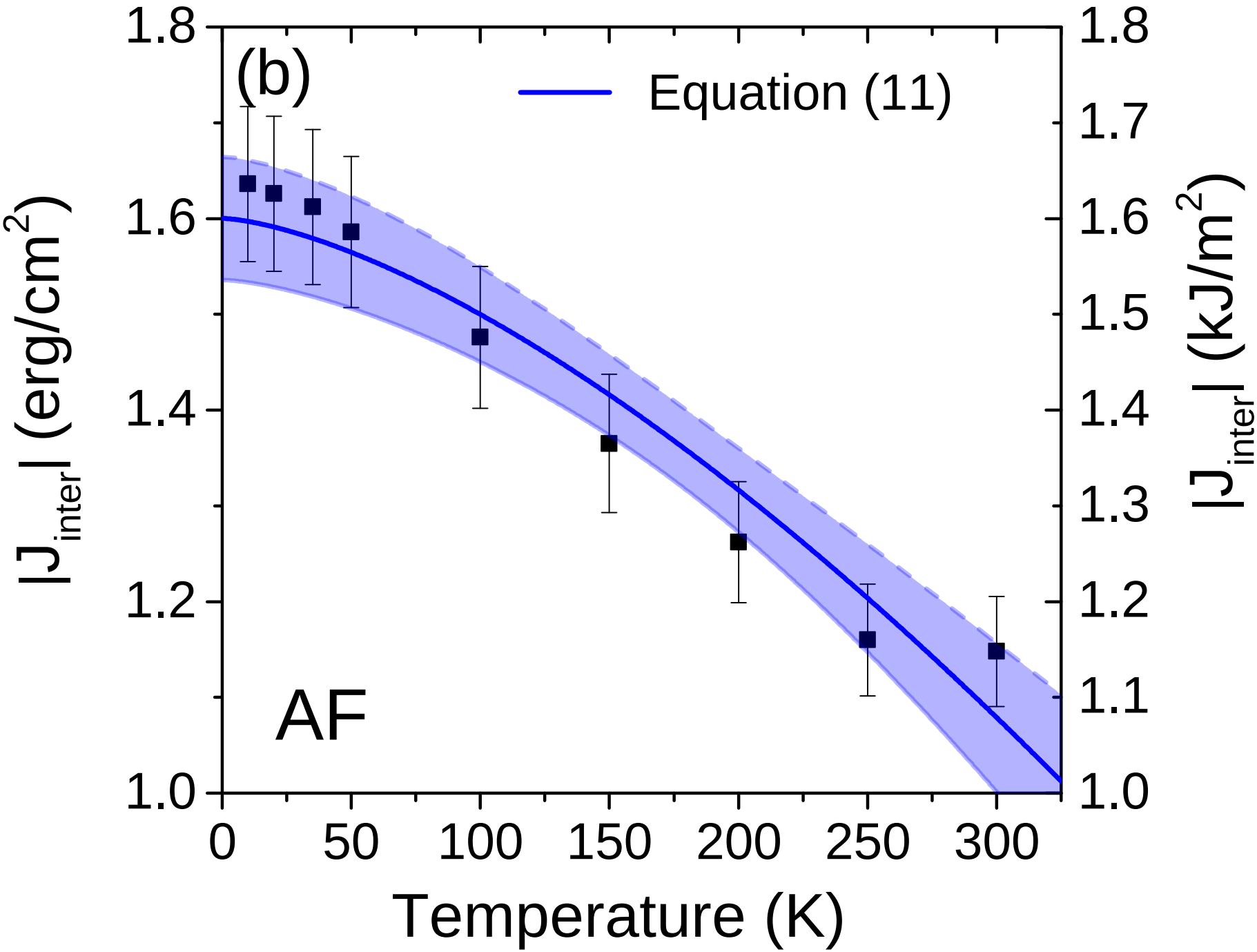
(b)
Equation (11)
AF
1.8
1.6
1.4
1.2
1.0
0
50
100
150
200
250
300
Temperature (K)
|J_inter| (erg/cm^2)
|J_inter| (kJ/m^2)
1.8
1.7
1.6
1.5
1.4
1.3
1.2
1.1
1.0

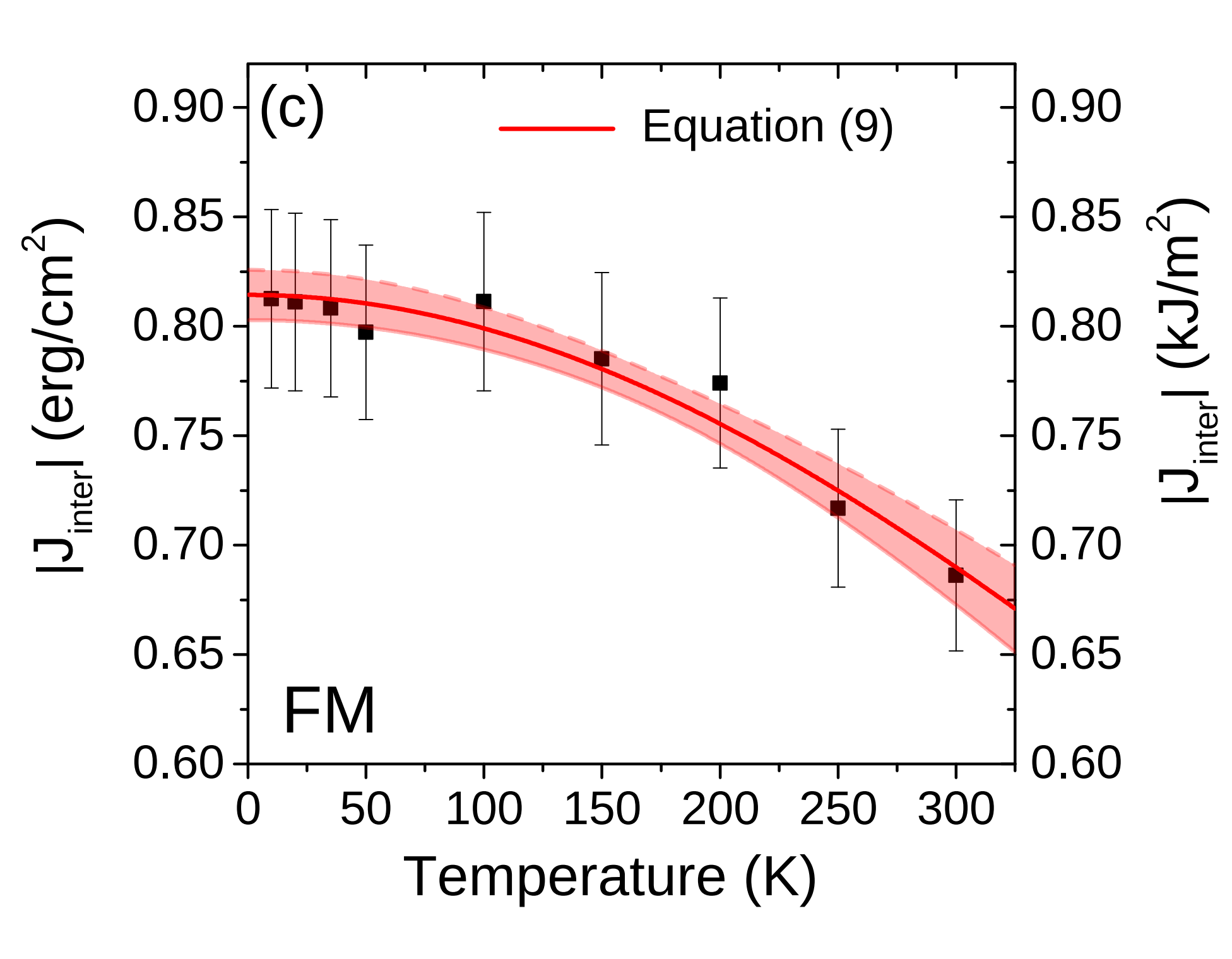
(c)
Equation (9)
FM
0.90
0.85
0.80
0.75
0.70
0.65
0.60
0
50
100
150
200
250
300
Temperature (K)
|J_inter| (erg/cm^2)
|J_inter| (kJ/m^2)

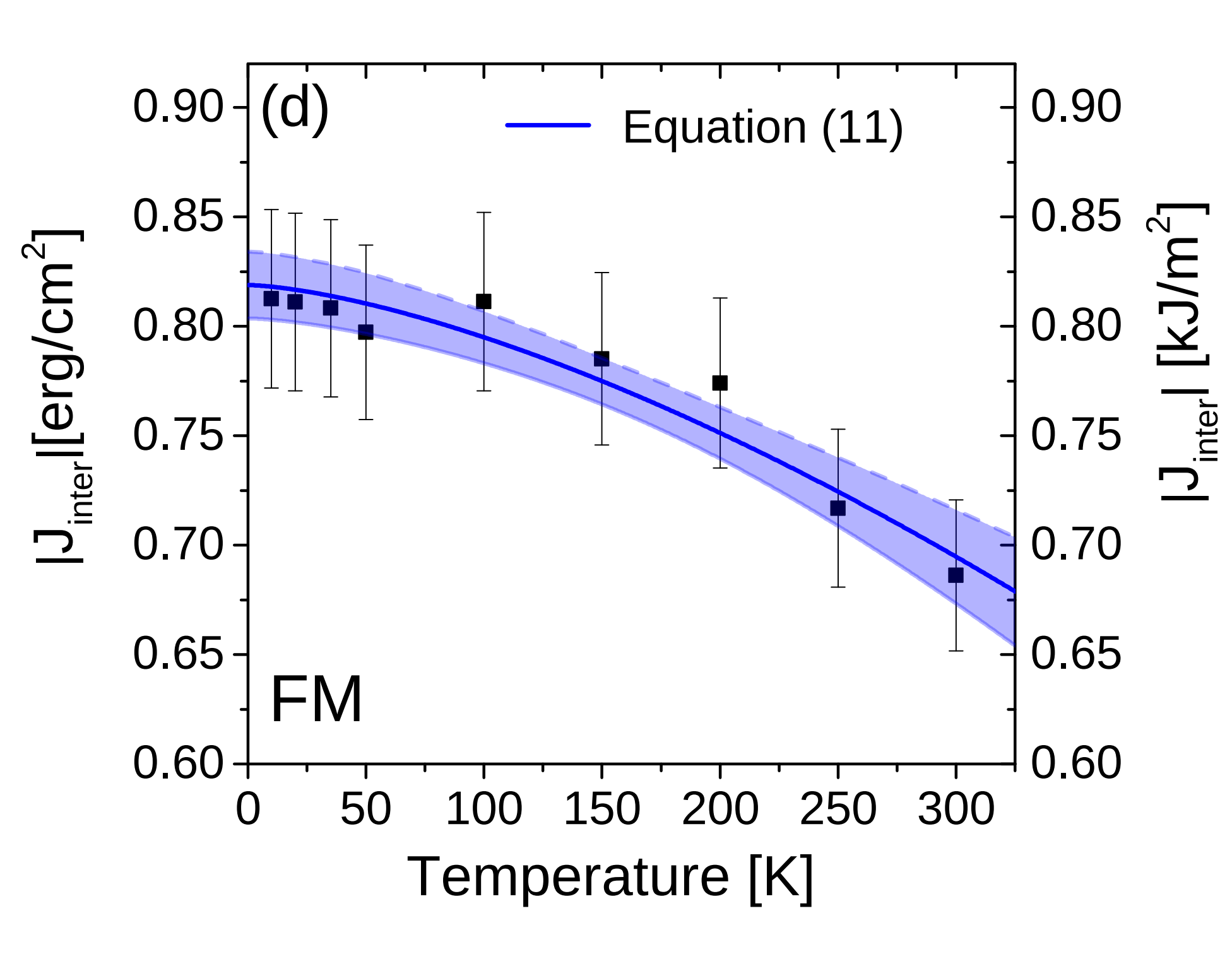
(d)
Equation (11)
FM
0.90
0.85
0.80
0.75
0.70
0.65
0.60
0
50
100
150
200
250
300
Temperature [K]
|J_inter|[erg/cm^2]
|J_inter| [kJ/m^2]

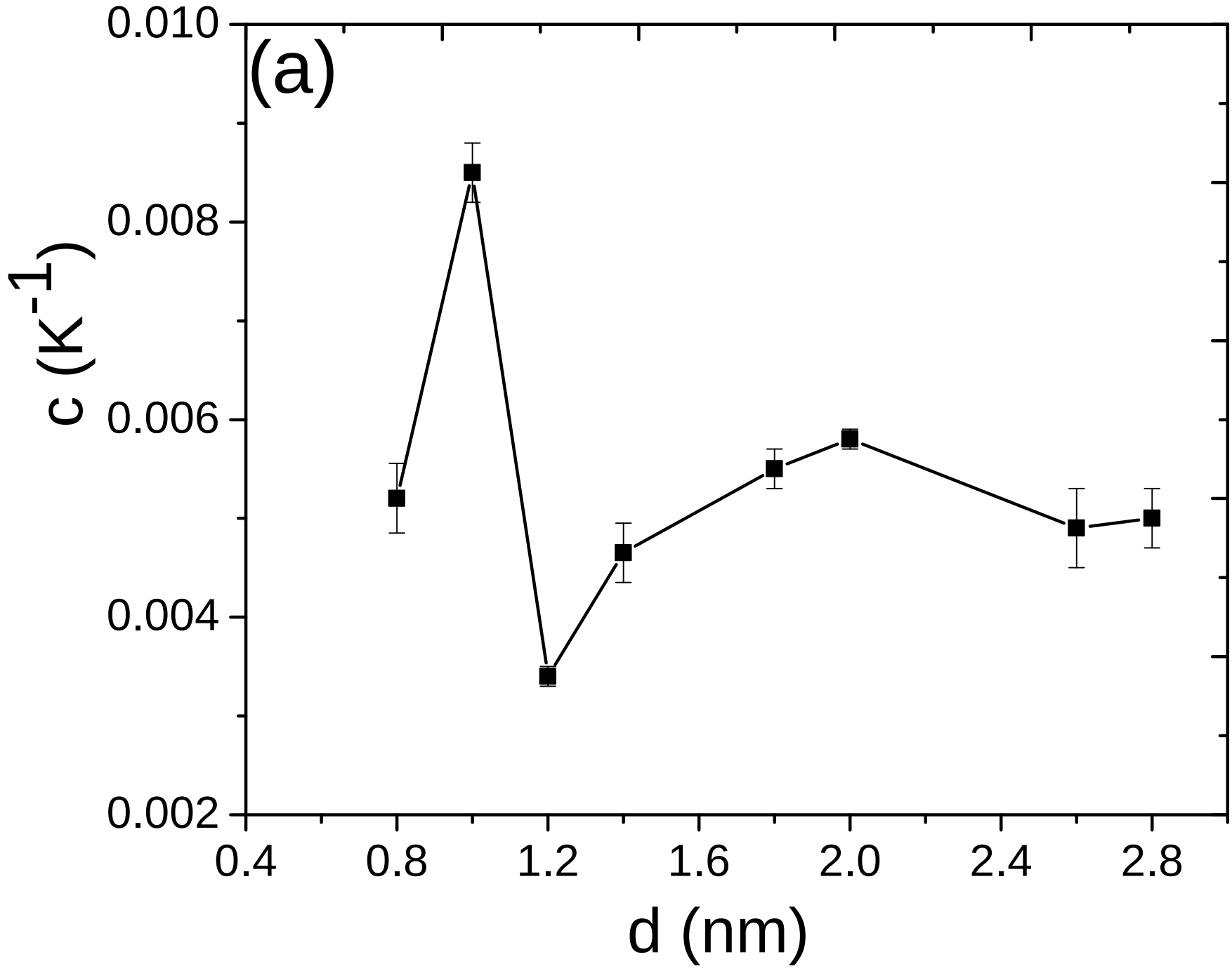
(a)
0.010
0.008
0.006
0.004
0.002
c (K-1)
0.4
0.8
1.2
1.6
2.0
2.4
2.8
d (nm)

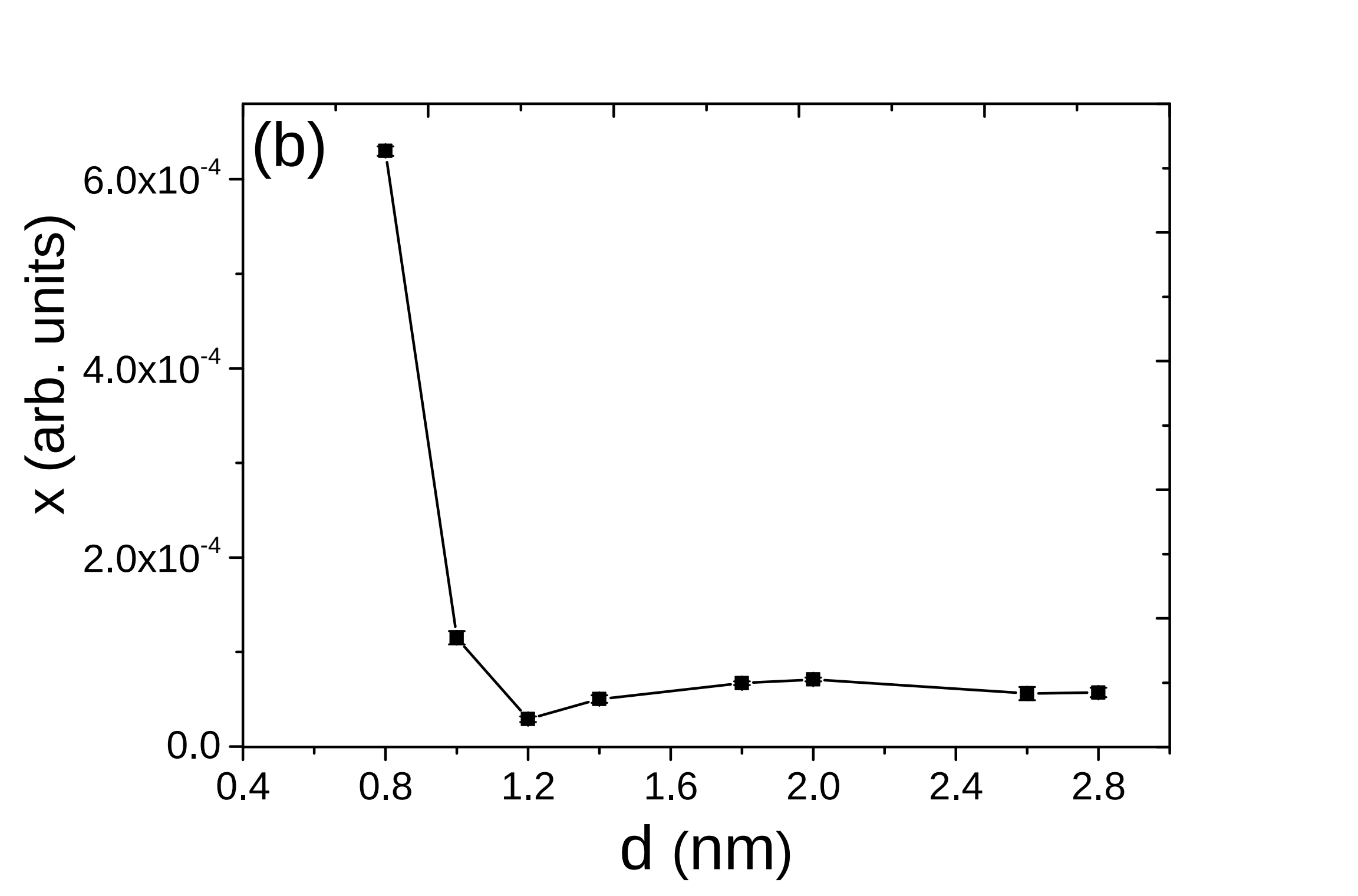
(b)
6.0x10-4
4.0x10-4
2.0x10-4
0.0
x (arb. units)
0.4
0.8
1.2
1.6
2.0
2.4
2.8
d (nm)